A computational approach to achieve uniform mechanical properties along the built-up direction in WAAM component

K Santhan Reddy

A Dissertation Submitted to
Indian Institute of Technology Hyderabad
In Partial Fulfilment of the Requirements for
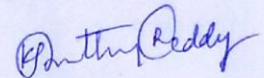The Degree of Master of Technology

भारतीय प्रौद्योगिकी संस्थान हैदराबाद
Indian Institute of Technology Hyderabad

Department of Mechanical and Aerospace Engineering

July, 2017

Declaration

I declare that this written submission represents my ideas in my own words, and where others' ideas or words have been included, I have adequately cited and referenced the original sources. I also declare that I have adhered to all principles of academic honesty and integrity and have not misrepresented or fabricated or falsified any idea/data/fact/source in my submission. I understand that any violation of the above will be a cause for disciplinary action by the Institute and can also evoke penal action from the sources that have thus not been properly cited, or from whom proper permission has not been taken when needed.
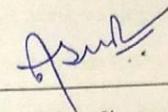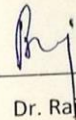
K Santhan Reddy

(ME15MTECH11012)

Approval Sheet

This thesis entitled 'A computational approach to achieve uniform mechanical properties along built-up direction in WAAM component' by K Santhan Reddy is approved for the degree of Master of Technology from IIT Hyderabad.
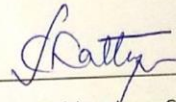
Dr. Abhay Sharma

Department of Mechanical and Aerospace Engineering

IIT Hyderabad

Adviser

Dr. Raja Banerjee

Department of Mechanical and Aerospace Engineering

IIT Hyderabad

Examiner

Dr. Subhradeep Chatterjee

Department of Materials Science and Metallurgical Engineering

IIT Hyderabad

Examiner

Acknowledgements

I would like to express my sincere gratitude to my supervisor Dr. Abhay Sharma, Associate Professor, Department of Mechanical and Aerospace Engineering, Indian Institute of Technology, Hyderabad for the support and guidance given throughout the research work.

I am very thankful to Mechanical and Aerospace Engineering staff for inculcating values and skills during the stay at IIT Hyderabad which are required for better living. I would like to thank Dr. Kazuhiro Ito, JWRI, Osaka University and Parchuri Pradeep, PhD student, Osaka University for their support in performing experimental investigations at Osaka university. I would also like to extend my Special thanks to Manish Kumar for moral and technical support.

Dedicated to

My Parents and all the Teachers

ABSTRACT

Wire arc additive manufacturing is a promising alternative to the conventional machining processes which builds large metallic components with low volume and medium complexity. However, its potential of higher deposition rate itself became the reason to bring large non-uniformity in mechanical properties at the bottom and top regions of the component. The reasons for this non-uniformity is the different cooling rates the portions of the component are undergone through. A finite difference model is developed to estimate the layer wise variation in thermal cycles and cooling times through which an understanding is developed on non-uniformity. To estimate the non-uniformity in mechanical properties, investigations are carried out on hardness. A hardness model is integrated with the developed thermal model to predict the layer wise hardness, estimating the non-uniformity along built-up direction. This hardness model is limited to certain range of mild steels. The experimental and simulation studies are performed on the single pass multilayer component. From experimental study, non-uniformity is observed in microstructures and the hardness values along the built-up direction. The simulated hardness values are in good agreement with the experimental one. Model is simulated under different process conditions such as maintaining constant baseplate temperature and diminishing the temperature of the heated baseplate according to the layer depositions. An understanding is developed to achieve uniform hardness along the built-up direction and a case is simulated proving it.

Nomenclature

T_s	Surface temperature
T_∞	Ambient temperature
h_{eff}	Combined convective and radiative heat transfer coefficient
Q_g	Heat generation rate per unit volume
$Q_{conv,rad}$	Convective and radiative heat loses
$K_{i,j,k}$	Thermal conductivity at position i, j ,k
$T_{i,j,k}$	Temperature at position i, j ,k
$H_{i,j,k}$	Enthalpy at position i, j ,k
ε	Emissivity
σ	Stefan Boltzmann coefficient
$\Delta x, \Delta y, \Delta z$	Element size in width, thickness and welding directions respectively
Δt	Time step
H^{n+1}	Enthalpy at current time step
H^n	Enthalpy at previous time step
η	Arc efficiency
V	Voltage
I	Current
Fo	Fourier number
α	Thermal diffusivity
n	Number of time steps heat source stays in one element
l1	Number of jumps heat source makes in one complete pass
l2	Number of jumps heat source makes in one-time step
hforced	Combined convective radiative heat transfer coefficient in forced cooling
hcoolant	Combined convective radiative heat transfer coefficient in coolant cooling
a, b	Variables
t1	Interlayer cooling time
TinP	Inter pass temperature
TinL	Inter layer temperature
n1, n2, n3	Number elements in width, thickness and welding directions respectively
n4, n5, n6	Number of divisions in width, thickness and length of an element respectively

CP	Specific heat
TP	Interpass temperature
TL	Interlayer temperature
t P	Interpass time
t L	Interlayer time
n	Number of time steps heat source stays in each element
n1	Number nodes along the deposited direction
nl, np	Total number of layers and passes respectively
Ti	Temperature of middle element in the ith bead
Tj	Temperature of middle element of middle pass in jth layer
t, tC	Time and cooling time respectively
j, i	Takes values from 1 to nl and np respectively
k	Takes values from 1 to number of nodes in a bead along the depositing direction
t n	Takes values from 1 to n
σ_y	Yield strength
d_g	Grain size
σ_0	Lattice resistance to dislocaation motion
k_y	Grain boundary resistance to dislocaation motion
CR	Cooling rate
A, n	Material constants
H_V	Vickers hardness
σ_y	Yield strength
m	Meyer's exponent
$T_{initial}$	Initial temperature of baseplate
T_{final}	Final temperature of baseplate
ΔT	Temperature change

Abbreviations

AM	Additive manufacturing
MAM	Metal additive manufacturing
WAAM	Wire arc additive manufacturing
CMT	Cold metal transfer
GMAW	Gas metal arc welding
GTAW	Gas tungsten arc welding
PAW	Plasma arc welding
Ni	Nickel
Ti	Titanium
Al	Aluminium
LENS	Laser engineered net shaping
SLC	Selective laser cladding
SLS	Selective laser sintering

CONTENTS

List of figures

List of Tables

Chapter 1

INTRODUCTION

Overview

In the present chapter, brief introduction of additive manufacturing and wire arc additive manufacturing are given where in challenges evolved and the need to investigate the thermal behaviour in wire arc additive manufacturing are discussed. Motivation behind the work and the overview of the thesis are also included in this chapter.

1.1 Additive manufacturing

Additive manufacturing(AM) is a promising technology that can fabricate complex geometry components with less human intervention and high material efficiency. According to American Society for Testing and Materials(ASTM), AM is ''a process of joining materials to make objects from 3D model data, usually layer upon layer, as opposed to subtractive manufacturing methodologies''. It has ability to fabricate single component structure with complex shape which is very challenging for other fabricating processes. Intricate and complex geometries can be manufactured with less post processing.

The materials used in these processes include polymers, metals, ceramics and biological systems [1]. In recent years, Additive manufacturing (AM) gained more importance in manufacturing industry due to its ability to produce complex parts directly from the Computer Aided Drafting(CAD) models reducing product development steps.

AM processes have the following advantages over conventional manufacturing technologies through which importance of AM can be realised,

- Material efficiency: AM manufacturing process have high material efficiency due to its ability to fabricate near net shape of the component by building layer by layer. Unlike, conventional manufacturing where large amount of materials need to be removed, AM mostly requires finishing operations.

- Resource efficiency: AM technology do not need any additional resources such as jigs, fixtures, cutting tools, and coolants that are must for most conventional subtractive

manufacturing. So, parts can be made by small manufacturers that are close to customers which results in improved supply chain dynamics.

- Part flexibility: There is no need to sacrifice part functionality for the ease of manufacturing, parts with complex geometry is possible in a single piece.

- Production flexibility: AM do not require additional resources like tool and component support systems which results small batch production more economical. Problems of line balancing and production bottlenecks are eliminated because complex parts are produced in single pieces. The quality of the parts depends on the process instead of operator skills due to which production can be modified easily according to customer demand.

- Environmental benefit: AM is environment friendly due to no material wastage and no tooling, making it a promising technology in all aspects.

AM technologies and methods grabbed the attention of various sectors such as automotive, medical, aerospace etc. Figure 1 represents percentage implementation of AM in various sectors. These technologies are implemented in motor vehicles and consumer products to greater extent.
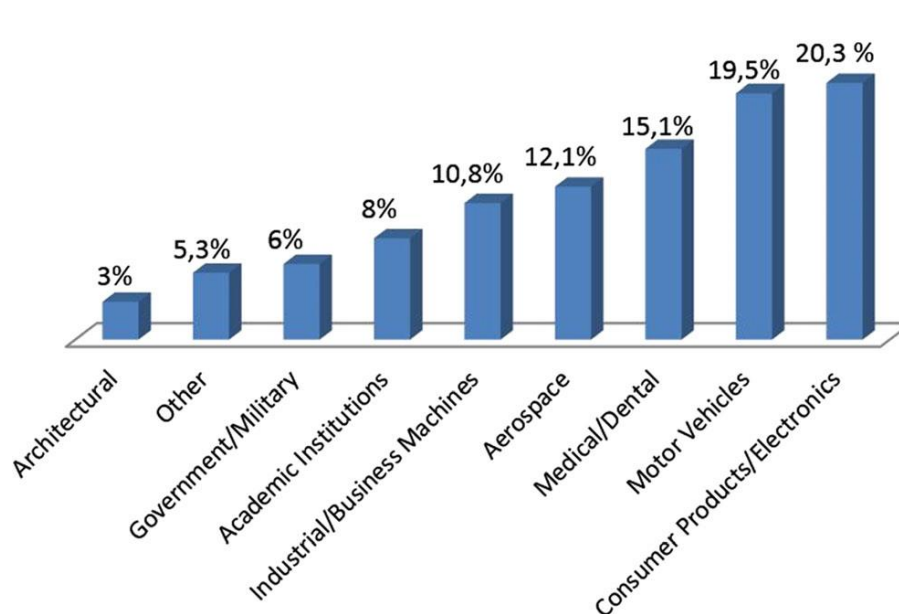
Fig.1 Sector wise implementation of AM process [2]

Nowadays, attention of AM is shifted to fabricate complex metal components to meet the demands of automotive and aerospace industries.

1.2 Metal additive manufacturing

Metal additive manufacturing (MAM) is an emerging technology with which complex metallic components can be manufactured that are very difficult to manufacture through conventional processes. Figure 2 gives an idea of the process of metal additive manufacturing. It can be classified on the basis of mode of material supply such as powder bed, powder feed and wire feed.

```
                    ┌─────────────────────────────┐
                    │  Metal Additive manufacturing │
                    └─────────────────────────────┘
            ┌────────────────────┴────────────────────┐
  ┌─────────────────────────┐              ┌──────────────┐
  │ Powder feed/Powder bed  │              │  Wire feed   │
  └─────────────────────────┘              └──────────────┘
      ┌──────────┴──────────┐        ┌──────────┼──────────────┐
  ┌──────────┐  ┌──────────────┐ ┌──────────┐ ┌──────────────┐ ┌──────────┐
  │Laser beam│  │Electron beam │ │Laser beam│ │Electron beam │ │Arc weld  │
  │based     │  │based         │ │based     │ │based         │ │based     │
  └──────────┘  └──────────────┘ └──────────┘ └──────────────┘ └──────────┘
```
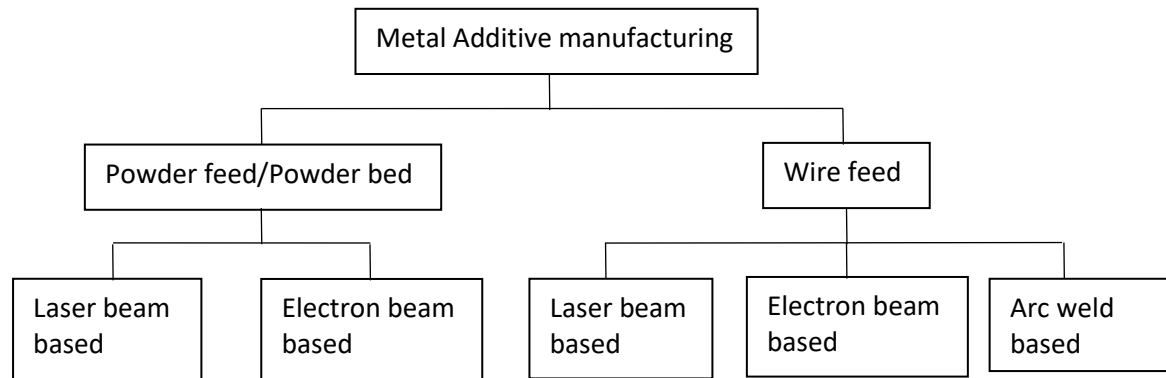
Fig.2 Classification of metal additive manufacturing

In Powder bed system, the powder is spread across the work area and sintered with laser or electron beam heat sources then next layer is sintered after spreading the powder over the previously sintered layer and this process is repeated till the desired part is achieved. Advantages of powder bed process are high resolution features, internal passages, and maintain dimensional control. In powder feed process, powder is deposited through the nozzle onto the substrate followed by heating and this process is continued to build the desired shape where as in wire feed process the molten material is deposited directly on to the substrate in the desired pattern and further layers are deposited over the previously deposited one achieving the final product.

Commonly used heat sources in powder based MAM are electron beam and laser based. Extremely small and highly complex metal parts can be manufactured, repaired or cladded using fine metal powders enabling with added functionality.

In comparison with wire feed process, powder feed process has ability to acquire higher dimensional accuracy and good surface finish. It is also capable of producing functionally graded materials [3].

However, metal powder based AM systems have the following backdrops compared to wire feed,

1. High specific cost due to low deposition rate and processing speeds

2. High capital cost of systems

3. Constraint of cost, quality and availability of consumables

4. Small build volumes

5. Mostly post processing is required due to poor material properties

Wire feed process has almost 100 % material usage efficiency that results in environment friendly and non-hazardous process. This wire feed technique also has benefits like less capital cost, low utilization cost of wire compared to that of powder feed technologies. Syed *et al.* [4] preformed a comparative study of wire and powder feed systems using laser heat source. Authors investigated the effects of these feeding techniques by fabricating a component which have five passes with 30% overlap and four layers deposited. Noticeable microstructural changes are not observed within the stainless-steel deposits in both feeding methods. Melt pool is more stable in wire feed compared to powder feed thus allowing for a better control of the weld pool shape. Wire feeding also be useful for cladding in various positions. For example, cladding of the inner wall of a tube can be achieved through wire feed technique [5].

In dependence with the type of source used for metal deposition, wire feed additive manufacturing is further classified into three groups, namely laser based, arc based, and electron beam based. Wire feed laser based AM is well known for producing high dense and precise components. Wire feed electron beam based AM is capable of depositing material at higher rates as well as lower rates. However, the energy efficiency of both laser beam and electron beam heat sources are very less compared to arc based source.
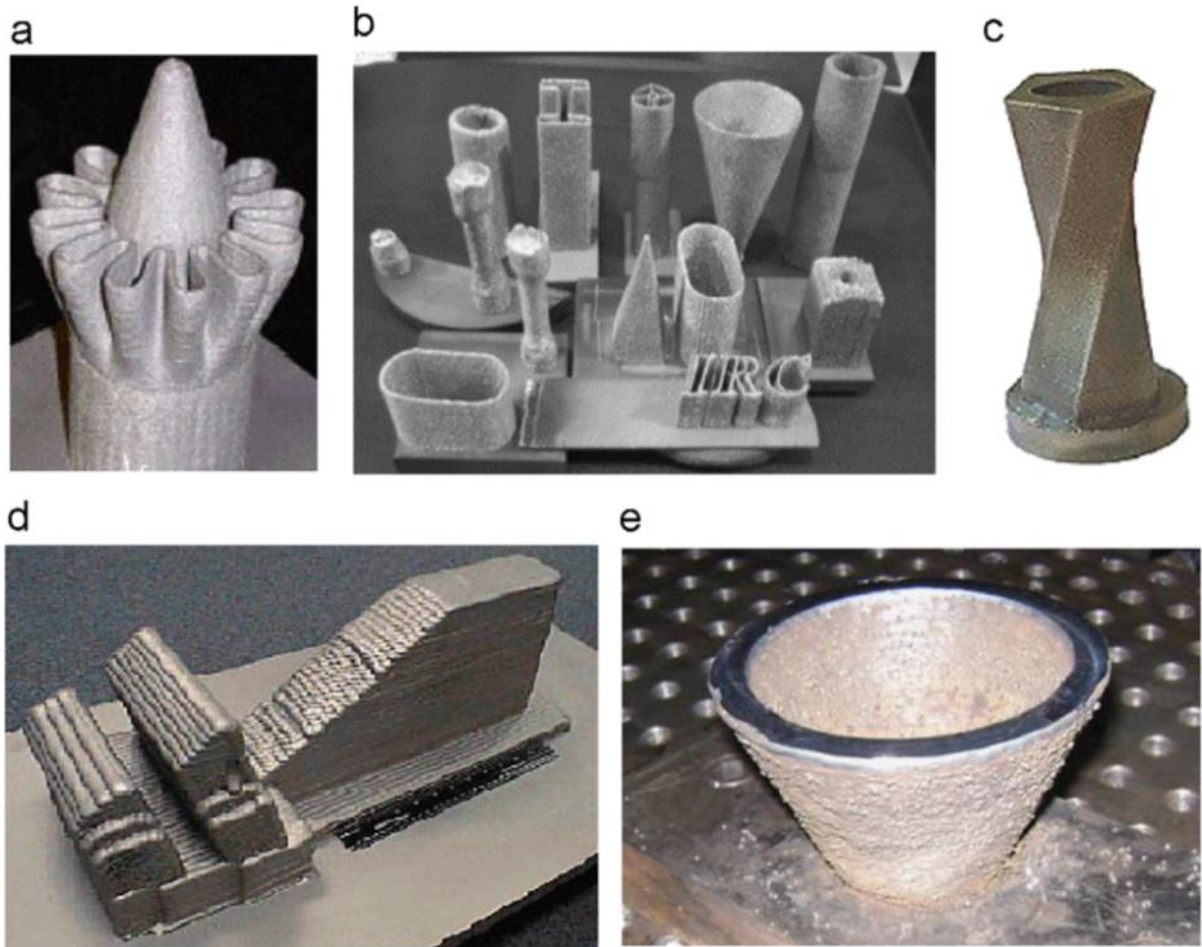
Fig.3 Comparison of surface quality of MAM process using laser based powder bed/feed (a and b), Electron beam based (c), laser based wire feed (d), and arc based (e) [6]

Table 1 Comparison between various MAM processes [7]

Source	Method	Resolution	Deposition rate	Power efficiency	Cleanliness	Cost Benefit	Surface finish
Laser	Powder bed	Excellent	Poor	Poor	Moderate	Poor	Excellent
	Wire	Moderate	Excellent	Poor	Poor	Poor	Moderate
Electron beam	Powder bed	Moderate	Good	Excellent	Excellent	Poor	Good
	Wire	Poor	Excellent	Excellent	Good	Good	Moderate
Arc	Wire	Poor	Excellent	Excellent	Poor	excellent	Poor

Surface quality of the components manufactured using different MAM techniques can be visualised in Fig. 3 where powder feed technique components are observed to have good surface finish. From the Table. 1, the suitability of WAAM to produce large metallic components can be realised. The present work is carried on WAAM, the process and, benefits and challenges of WAAM are discussed elaborately in the following section.

1.3 Wire arc additive manufacturing

The metal AM technique with the combination of wire feed and arc based heat source is well known as wire arc additive manufacturing (WAAM). Figure 4 explains the basic principle involved in WAAM where heating of electrode/filler metal through arc and depositing on the substrate. WAAM process uses gas metal arc welding (GMAW), gas tungsten arc welding (GTAW) or plasma arc welding (PAW) techniques for the deposition of molten metal. GMAW is more advantageous in technical and economic aspects when compared with GTAW. The production rate of GMAW is high due to higher deposition rate. GMAW has co-axial consumable electrode which is perpendicular to the weld. Unlike GMAW, GTAW and PAW uses non-consumable electrode due to which the care need to be taken for the wire feed orientation resulting the process complicated. However, the major problem in GMAW are arc instability and severe spattering conditions that results in imprecise weld bead placement. Cold metal transfer (CMT), a modified gas metal arc welding variant based on controlled dip transfer, used widely for WAAM processes due to its high-quality beads, low heat input and almost no spatter [8].
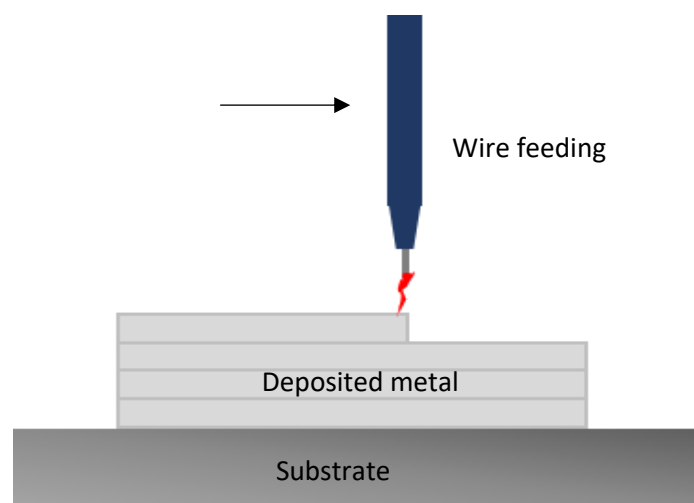
Fig.4 WAAM process principle

WAAM has its own advantages such as higher deposition rate, energy efficient, low part cost and high material efficiency. Various weldable metals like steel, Ni alloy, Ti alloys and Al alloys [9] can be used to fabricate components. Metal deposition rate ranges from 1kg/hr to 4 kg/hr [9]. Higher deposition rate processing of WAAM made easy to fabricate large metallic components. This manufacturing process is considered to have high material efficiency which reflects better buy to fly ratio and low part cost. Figure 5 shows some components manufactured by WAAM process using GMAW.
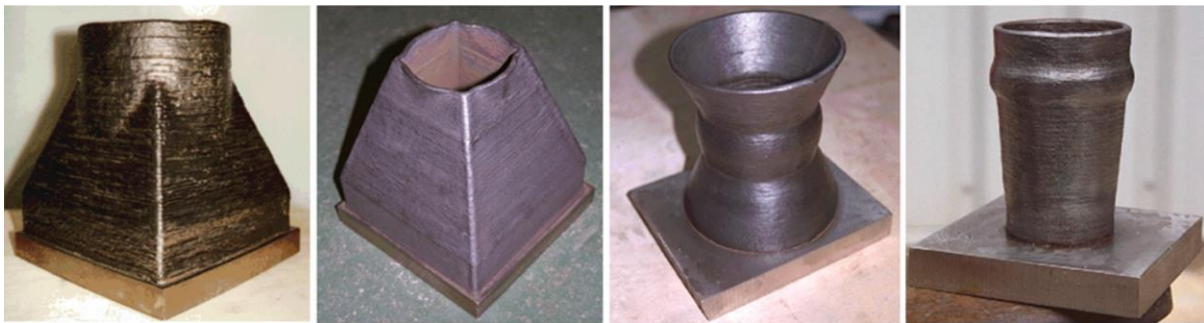
Fig.5 Metal components produced by WAAM process [9]

Besides these benefits, WAAM process have some technical challenges yet to be resolved which includes,

1. Residual stress and distortion
2. Non-uniform properties in built-up direction
3. Stair stepping effect and
4. Poor surface finish.

The main reason for evolving these challenges is the repetitive thermal cycles that a component undergoes through. This thesis mainly focusses on understanding and resolving the non-uniform mechanical properties along built-up direction.

The non-uniformity along the built-up direction is due to the different cooling rates that various portions of the component undergoes due to repetitive thermal cycles. Therefore, a numerical tool is required to assess the thermal cycles and the hardness of the WAAM component. Thus, the main aim of the present work is developing a simple tool which can predict the hardness variation and to propose a methodology to bring the uniformity in mechanical properties along the built-up direction.

1.4 Motivation

Even in this technologically advanced era, manufacturing metallic complex parts is still remained as a challenge while controlling both economy and manufacturing time. WAAM is a technology which has ability to manufacture large parts with medium complexity with high material efficiency that meet the requirement. Mostly the research is undergoing on the challenges like residual stress formation, deformation and surface finish, paying less attention in addressing non-uniform mechanical properties along the built-up direction. Few research groups carried investigations experimentally to understand the property variations but the ways to reduce non-uniformity is unanswered. A tool is required to predict any mechanical property for a component manufactured using WAAM process, thereby assessing property variation along the built-up direction. Predicting hardness is one of the best ways to estimate the property variation. Cooling rate is required as one of the inputs to assess the hardness which shows the need to develop a thermal model for the WAAM process. So, the thermal model with hardness prediction gives the solution to assess the non-uniformity and a chance to simulate various process condition to develop understanding in achieving uniform mechanical properties.

1.5 Overview of thesis

Chapter 1: Introduction

In this chapter, brief introduction of AM, MAM and WAAM, and the challenges facing by researchers with WAAM are discussed.

Chapter 2: Literature review and problem statement

In this chapter, various researchers undergone in WAAM and various models developed for understanding the process and the challenges that are available in literature are presented. Also, discussed the gaps and opportunities present in this field. Problem statement and the objectives are stated based on the gaps and opportunities.

Chapter 3: Thermal modelling

In this chapter, technique used for discretising the 3D heat conduction equation and various modelling aspects like meshing strategy, time marching and stretch transformation are discussed. Hardness model also discussed briefly in this section.

Chapter 4: Experimental details

This chapter gives information about the experiment and the implementation of various cooling strategies to manufacture a thin walled component using WAAM.

Chapter 5: Results and discussions

In this chapter, the thermal cycles, cooling times, $\Delta t_{8/5}$ are extracted for different layers are presented and predicted the hardness variations. The experimental outcomes like microstructures and hardness for different cooling strategies are discussed. Methodology to bring out uniformity is also investigated and presented in this chapter.

Chapter 6: Conclusions and future work

In this chapter, the conclusions brought from the results and discussions are stated. Also, discussed the direction for the future work.

Chapter 2

LITERATURE REVIEW

Overview

The present chapter briefs about the evolution of WAAM and various studies describing the challenges WAAM facing to utilise the component in practical situations. Various thermo-mechanical models and modelling strategies that are developed to investigate the thermal behaviour and, prediction of residual stresses and distortion of WAAM component are presented. From the study of literature, gaps and opportunities are observed and are summarised in this chapter.

2.1 Background

The first patent of WAAM was filed in the year 1925 by baker [10]. In this patent process of manufacturing the objects using an electrode to deposit material in fused is discussed. Figure 6 shows the objects manufactured using this technique. This process was not automated and fully depend on the skill of the operator in handling the welding torch.
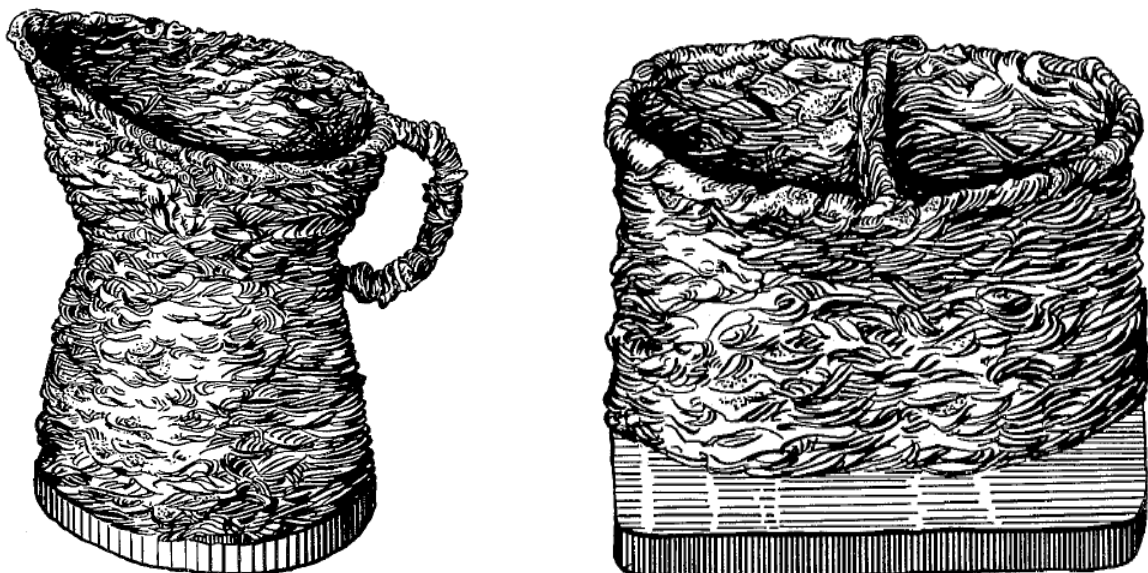

Fig.6 Examples of the objects manufactured firstly using manual weld deposition technique [10].

In 1925, Eschholz [11] found that the arc current, travel speed, bead width, bead height, base material and penetration depth as process parameters for this process. Shockey understood that the welding speed and current shows influence greatly on the geometry of the deposited bead [12]. Carpenter and Kerr investigated that preheating resulted a higher deposition rate using a submerged arc welding technique [13]. Dickens et al. [14] performed a preliminary study of additive manufacturing using GMAW techniques. Researchers understood the significant advantage of process combining with a commercial robot when compared to conventional techniques. Shaped metal deposition [15] process, an application of WAAM process, showed its capability of building large reactor components where the components retained approximately 80% of the unmachined weight that gained a huge benefit comparing the 28% effective weight by the traditional forging process. Even though the first patent is filled long back, the investigations are happening extensively from past 30 years only, because of the availability of modern welding and automation technologies. Literature review on WAAM is broadly classified on the basis of investigations carried upon to encounter the various challenges while performing WAAM process as follows,

- Residual stresses and distortion
- Surface Roughness and stair stepping effect
- Mechanical properties variation

2.2 Residual stresses and distortion in WAAM

In general, the formation of residual stresses and distortions are due to the thermally induced strains which are formed because of non-uniform expansion and contraction a material undergoes. These strains disappear either by distorting the material or by microscopic deformation which results in yielding otherwise residual stress formation. Formation of residual stress is a major concern especially while fabricating large scale components through WAAM. If the component is unclamped the residual stresses results in distortion of the component. High heat input and repeated thermal cycles through which component undergoes in WAAM results in the formation of residual stress. Currently following methods are used to reduce residual stress and distortions formed in the component [16].

- Symmetry building: In this method, substrate will be coincided to the plane of symmetry of the component volume and the deposition is carried on the opposite sides so as to balance the stresses formed.

- Back to back building: Two components are manufactured simultaneously on the opposite side of the substrate where substrate is not the part of a component. Before separation the parts are heat treated to dissipate the residual stresses.

- Optimising part orientation: Residual stresses can be less for depositing the shorter layers. Considering this, component can be fabricated in the direction perpendicular to the longest length. In some cases, it may be impractical because of more numbers of stops and starts.

- High pressure interpass rolling: By interpass rolling residual stresses can be reduced along with the microstructural advantage. The peak stresses are reduced at the interface between the component and the substrate whereas compressive stresses are induced in the top layers.

Even though these processing techniques are available to reduce residual stresses, complete elimination of residual stresses is not possible through this. Various studies are developed to minimise them in the processing stage itself. Many researchers investigated the effects of inter pass cooling time, deposition patterns and the depositing directions to minimise the formation of residual stresses as described in the next section.

2.2.1 Thermal and mechanical models

Zhao [17] investigated the effect of interpass idle time and the depositing directions in weld based AM with the help of 3D FE analysis and concluded it as a significant parameter to control residual stresses. The author also concluded that the deposition of last layer has considerable effect on the residual stress formation in the work piece. Various thermomechanical models are proposed to estimate the residual stresses and study the effects of various parameters. The effects of continuous and interpass delay deposition, and depositing directions on residual stress is studied by Mughal [18], [19] developing two-dimensional (2D) finite element(FE) thermomechanical model. The continuous deposition results in greater preheat temperature that reduces deflection in comparison with case providing inter pass time but with continuous deposition temperature of the baseplate

increases resulting lower process efficiency. So, in order to avoid tolerance loss certain interpass time may be required. The author also developed a 3D FE model to study the effect of bolting [19] on residual stress formation in single layer multi pass.Nickel [20] investigated the effect of deposition patterns over the residual stresses by developing a FE model. From this it can be understood that the parameters like interpass idle time, depositing directions and the deposition pattern shows considerable effects on the thermal cycles because of which the high residual stresses are formed.Ye et al. [21] developed a numerical model for single bead wall from which temperature distribution and the gradient are predicted and described the potential of simulated thermal history. 3D finite element thermal modelling for direct laser fabrication is proposed by Yang and Wang [22] by which thermal history of melted pool and the whole model can be predicted. The investigation of the dynamically changing substrate geometry is carried out by Jandric and Kovacevic [23] using FE thermal simulations, where a significant influence on the molten pool geometry and heat transfer condition is observed which affect quality of the WAAM product. Peyre et al. [24] developed a two-step thermal simulation to predict the shapes of manufactured structures and thermal loadings induced by an Selective laser cladding(SLC) process. An analytical model together with a FE model is utilised by Alimardani et al. [25] to predict the final geometry of the walls and the thermal behaviour of the deposition process. Charles [26] developed a microstructure model for Ti-6Al-4V which can be coupled to a thermo-mechanical model of the metal deposition process.

In the metal AM, thermally induced stresses and distortions are analysed using sequentially coupled thermo-mechanical models. Chin et al. [27] generated a 1D and a 2D FE model for a thermo-mechanical study of the temperature and stress distributions of metal AM process on a droplet level by using a single molten metal droplet onto a comparatively large substrate. It is found that localised preheating by previously deposited droplets does not significantly affect final stress distributions after deposition of a second droplet on top of the first droplet. The residual stress study on multi-layered part and successive deposition of a column of molten metal droplets on a large substrate which further proved that the localised preheating by previously deposited material is not effective in reducing thermal stresses [28]. The high temperatures in newly deposited material relieves stresses in the existing adjacent deposited layers. Hence, existing stress states in previously deposited layers cannot significantly affect the final residual stress distributions in subsequent layers. Chin et al. [29] observe the limited

thermal interactions in the models with successive deposition of adjacent droplets in a row on a relatively large substrate. However, the results for molten material droplets on a thin substrate showed that the preheating effect can reduce thermal gradients of the parts and substantially reduce the residual stress magnitudes. The same effect is expected for deposition of a large number of droplets on a thicker substrate. This self-generated stress reduction from the deposition process could be increased by choosing optimal deposition paths.

2.2.2 Thermal mechanical model strategies

Transient thermo-mechanical models are widely used to solve welding problems creating a real-life situation to understand the various effects. However, high computation time and memory allocation is the major concern for these models. Many computationally efficient approaches are developed with time, solving the major issues involved in these models. These approaches can be categorised as, which are reducing the model size by using simplified meshes and solving the problem with static analysis.

Different meshing strategies like graded meshing, adaptive meshing, sub structuring [30] etc., are used to reduce the number of nodes/elements while achieving good accuracy. Graded meshing strategy is widely used in welding process [17, 19] modelling where the beads are meshed finely and the regions which are away from the bead are made coarse.
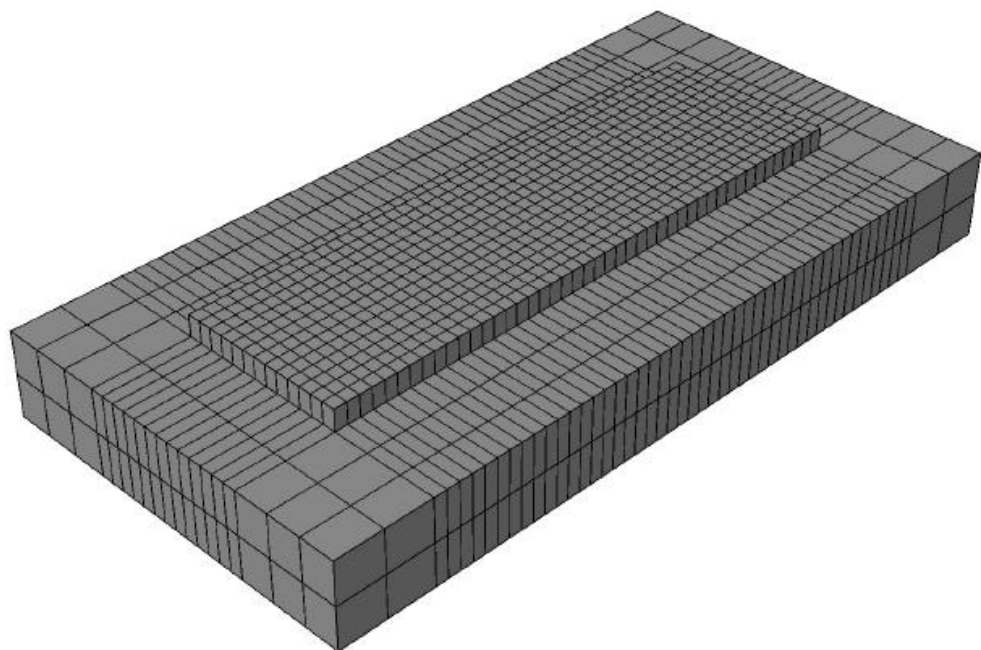

Fig.7 Graded meshing model [19]

Figure 7 shows the model developed for thermal analysis of weld based rapid prototyping by Mughal where multiple beads are deposited over the substrate and the beads are maintained finer comparatively. A computationally efficient model is developed for large wire arc additive manufactured components by Ding et al. [31] using steady state thermal model to predict the thermal profiles in the process. Comparison of computation time and the effective predictability between steady state and transient thermomechanical models is made. Transient method that uses Lagrangian approach where time increment scheme is used to model moving welding torch. Steady state method uses eulerian approach where welding torch is steady and the material is moving through the mesh. As the steady state model, does not require dense mesh, this will be computationally efficient compared to transient approach. Both the approaches predict the thermal history equally good. The computation times for thermal and mechanical models simulated under transient and steady state approaches are shown in Table 2.

Table.2 Computational time comparison between transient and steady state approaches [31].

	Thermal analysis time	Mechanical analysis time	Total analysis time
Transient model	51hr 24min	24hr 1min	75hr 25min
Steady state model	10min	14hr 46min	14hr 56min
Time saving (%)	99.69	38.51	80.21

However, there is certain limitation for eularian approach with the part length. This approach cannot be used to study the short parts as it assumes that the part is infinitely long. The minimum length of eularian model is dependent on the problem and it should be long enough to achieve steady state [32]. Most of the available models utilise transient approaches to simulate layer depositions.

Michaleris [33] developed finite element method for heat transfer analysis of laser engineered net shaping (LENS) manufacturing by reviewing two depositing techniques namely quiet element method and inactive element method. In quiet element method, all the elements i.e., active and inactive elements are participating in the analysis all the time but the properties of inactive elements are assigned in such a way that their effect can be neglected. As the number of elements participating in the analysis will not change, there is no requirement of renumbering and solver initialization. Hence, this method is easy to implement but takes long number of runs. In inactive element method, the inactive elements are removed from the analysis considering only active elements. The number of runs required will be less as solver has to analyse only active elements. But, renumbering and solver initialization is required which may increase the computational time. A new hybrid quite inactive method is proposed by the author in which initially all the elements are set inactive and switching layer by layer to quiet. A single pass sixty-two-layer model is analysed under these three deposition techniques and found that computational time is comparatively less for hybrid inactive quiet technique. However, the inactive element method would be computationally efficient without renumbering and solver initializations. Zhao [34] developed a three-dimensional finite element thermal model to investigate thermal cycles, temperature gradient and the effect of depositing directions. Dense mesh is used in the cladding and sparse mesh away from it because of which number of nodes are reduced that shows positive effect on computation time.

2.3 Surface Roughness and stair stepping effect investigations

The profile or the shape of the weld bead that is deposited would be near to parabola. In WAAM the component is fabricated with many such beads which results in unevenness of the final surface. The effect of various process parameters namely wire feed speed, welding speed, wire diameter, voltage and contact tip to work distance on the bead geometry and wall thickness are investigated by Dickens et al. [35]. In this study, the wire feed speed and wire diameter are found to have a positive effect on width and height of bead, whereas welding speed has a negative effect. Wider and thinner weld beads are seen with increased voltage. Various investigations are carried out on the strategies like controlling bead geometry with process parameters and overlapping beads methodology to achieve better

surface finish of the component. Song and Park [36] and Karunakaran et al. [37] studied various welding AM and milling techniques to improve surface quality and the accuracy of the manufactured components.

Researchers developed multiple beads overlapping models, correlations between process parameters and the bead geometry to control surface finish. Aiyiti [38] developed an overlapping model to predict appropriate overlapping parameters for better mechanical properties. Suryakumar [39] modelled the bead cross-section with the parabola. Cao [40] found that the sine profile gives the best fit compared to other profiles namely gaussian, logistic and parabola. Xiong [41 ,42] proposed that the optimal model depends on ratio of wire feed rate to welding speed by fitting different profiles like parabola, circular arc and cosine with the bead cross-section that are deposited under various welding parameters. In WAAM, heat develops excessively in local area due to continuous deposition, causing more re-melting of the previously deposited layers leading to poor dimensional tolerances [43].

2.4 Microstructure and mechanical properties

Research mostly undergoing in addressing the effects of process parameters on residual stress and surface finish paying less attention to control non-uniformity in mechanical properties along the built-up direction. Attempts are made to understand the variation of mechanical properties in WAAM components giving less efforts in controlling them.

Martina [44] showed that mechanical properties can be improved by inter pass rolling the WAAM component. In WAAM, the repetitive heating and cooling cycles undergone by the component as a part of fabrication is the main reason for anisotropic microstructure along the built-up direction. The mechanical properties like tensile strength, hardness is directly influenced by the microstructural features of the component thereby exhibiting non-uniform mechanical properties. The bottom layers of the component undergo more thermal cycles compared to top one's leading to softening [21]. So, the hardness is considerably high for top few layers compared to the bottom layers [45] resulting in non-uniformity in mechanical properties. Brandl [46] studied the effects of heat treatments over the microstructure and hardness of wire feed AM titanium alloy component. Even though the research work carried on titanium alloys the effect of repetitive thermal cycles on the lower and upper beads can be understood.

It is reported that the hardness values decrease from first deposited layer and then increases towards top layers for steel AM component. This non-uniformity is due to different cooling rates and repetitive heating cycles.

Costa [47] developed a thermal model for laser powder deposition through which thermal history is predicted. From the thermal history, high cooling rates are observed in laser processing due to which the diffusive transformations of austenite are suppressed totally and undergoes only martensitic transformation as it cools down to room temperature. Hardness values are predicted considered the existence of only two phases in the component.

The transformation and formation of microstructure of steel component manufactured using laser engineering net shape deposition are discussed briefly by Kadiri [48] and the hardness variation along the built-up direction is investigated.

Zeng [49] examined the tensile strength and hardness values of laser engineered net shaping component. The effect of thermal history over the microstructure evolution is analysed.

Manvatkar [50] developed a 3D thermal model for LENS component from which cooling rate are extracted and are utilised to estimate hardness and tensile strength values. Hall-Petch relation is used to predict tensile strength as shown in Eq. 1

$$\sigma_y = \sigma_0 + k_y(d_g^{-1/2})$$ ……………………………………. (1)

where,

σ_y − yield strength

d_g − grain size

σ_0 − lattice resistance to dislocaation motion

k_y − grain boundary resistance to dislocaation motion

But in the present study d_g is considered as cell spacing and is calculated from the cooling rate, which is given by

$$\lambda_2 = A(C_R)^{-n}$$

Where, C_R is cooling rate and A, n are material constants.

Hardness is calculated from the yield strength which is given by,

$$H_V = 3\sigma_y(0.1)^{2-m}$$

Where, H_V is hardness in kg/mm^2, σ_y is yield strength in kg/mm^2 and m is meyer's exponent

This model over estimates the hardness which is measured along the built-up direction.

It is understood from the above discussion that there are few finite element models developed for the investigation of thermal behaviour of WAAM. As the finite element method is computationally expensive, the model will be limited to less number of layer /and passes. The finite difference method is advantageous compared to finite element method in the aspect of visualising the physics behind the process and computationally efficient in handling simple geometry. Accuracy in finite difference model can be achieved by acquiring finer details in the region of high thermal gradient. So, a model can be developed implementing finite difference method assuming temperature dependent properties for simple geometry. The lack of control over the cooling rates and the thermal cycles encountered by different layers in the fabrication process, results in inconsistency in the properties of the components along the build direction. So, controlling cooling rates plays a significant role in product quality which can be achieved in two ways. One way is by controlling process parameters like heat input, interpass time etc., and the other is by introducing backing plate, creating controlled environment and controlled heating baseplate. To understand the effect of various process parameters and other cooling/heating strategies on the mechanical properties of the component a tool need to be developed through which an approach to bring uniformity can be realised.

2.5 Scope of Work

The non-uniformity in the mechanical properties along the built-up direction is one of the important areas to address. The thermal cycles undergone by the component are the key reason for this non-uniformity. So, thermal model need to be developed to understand the effect of deposition of new layers over already deposited one. A predictive model for mechanical properties is to be developed to assess the variation along the built-up direction. The flexibility to change various process parameters in this model is needed to understand the effects of those parameters and the conclusion or the methodology can be obtained to achieve the uniformity in mechanical properties.

2.6 Problem statement and objectives

'A computational approach to achieve uniform mechanical properties along the built-up direction in WAAM component'

For better understanding of layer effect on thermal profiles and mechanical properties, there is a need to analyse a model with more number of deposited layers. However this may become computationally expensive in handling. So, a simpler code is required with possibility of changing welding parameters with layers to assess layer effect and thermal history. Thus, objectives of the work are to

1) Develop a computationally friendly model for WAAM which can handle multi-layer multi-pass scenario, changing parameters with passes, inter-pass temperature, inter pass time.

2) Understand thermal behaviour with increasing number of layers and its effects over microstructure and hardness.

3) Develop the understanding on the effect of layer deposition over preheated baseplate on mechanical properties specifically hardness.

4) Propose a scheme to control cooling rate which brings uniform mechanical properties along the built-up direction of the component.

Chapter 3

Modelling

overview

This chapter is broadly classified into two major parts namely thermal model and the hardness model. In thermal model numerical formulations, meshing strategy, time marching, assumptions and boundary conditions are discussed. After which the modelling approach of hardness model is explained briefly. Later, the overview on integrated model i.e., thermal and hardness model, and the flow chart of the thermal modelling approach are presented.

3.1 Thermal model

3.1.1 Numerical Formulation

Fourier heat conduction equation is used in enthalpy form in which convective-radiative heat losses and heat loss/gain during phase change are also included as shown in Eq. 2. Finite difference method is used to discretise the equation in terms of space [51].

$$\nabla.(K\nabla T) + Q_g - Q_{conv, \ rad} + Q_{Latent} = \frac{DH}{Dt} \qquad \text{........................ (2)}$$

In finite difference method, model is divided into control volumes and each control volume bares a node at its geometric centre. Equation 2 is discretised in space, transforming partial differential equations to ordinary differential equation. Thermal conductivity which is considered as temperature dependent is calculated at the interface of two nodes is given by the harmonic mean of their thermal conductivity which ensures heat flux continuity as shown in Eq. 3.

$$K(T1, T2) = \frac{2}{\frac{1}{K(T1)} + \frac{1}{K(T2)}} \qquad \text{.................................... (3)}$$

Central difference method is used to discretise in space. The rate of change of enthalpy for any node can be given by Eq. 4.

$$\frac{DH}{Dt}_{i,j,k} = \{2K_{i,j,k}\}\left\{\begin{array}{l} \dfrac{K_{i+1,j,k}\left(T_{i+1,j,k} - T_{i,j,k}\right)}{(K_{i+1,j,k} - K_{i,j,k})\Delta x^2} + \dfrac{K_{i-1,j,k}\left(T_{i-1,j,k} - T_{i,j,k}\right)}{(K_{i-1,j,k} - K_{i,j,k})\Delta x^2} \\[3mm] + \dfrac{K_{i,j+1,k}\left(T_{i,j+1,k} - T_{i,j,k}\right)}{(K_{i,j+1,k} - K_{i,j,k})\Delta y^2} + \dfrac{K_{i,j-1,k}\left(T_{i,j-1,k} - T_{i,j,k}\right)}{(K_{i,j-1,k} - K_{i,j,k})\Delta y^2} \\[3mm] \dfrac{K_{i,j,k+1}\left(T_{i,j,k+1} - T_{i,j,k}\right)}{(K_{i,j,k+1} - K_{i,j,k})\Delta z^2} + \dfrac{K_{i,j,k-1}\left(T_{i,j,k-1} - T_{i,j,k}\right)}{(K_{i,j,k-} - K_{i,j,k})\Delta z^2} \end{array}\right\}$$

$$+ \; Q_g \; - \; Q_{conv, \; rad} + \; Q_{Latent} \qquad\qquad\text{............................. (4)}$$

where,

Q_g represents volumetric heat generation rate

$Q_{conv, rad}$ represents volumetric heat convective and radiative losses rate

Q_{latent} represents heat lost or gained in phase change (liquid $\Leftrightarrow$ solid)

The ordinary differential Eq. 4 is solved in time using fourth order Runge-Kutta technique,

$$H_1 = f^n(H)$$

$$H_2 = f^n\left(H + \frac{\Delta t \cdot H_1}{2}\right)$$

$$H_3 = f^n\left(H + \frac{\Delta t \cdot H_2}{2}\right)$$

$$H_4 = f^n(H + \Delta t \cdot H_3)$$

$$H^{n+1} = H^n + \Delta t \cdot \left(\frac{H_1 + H_2 + H_3 + H_4}{6}\right) \qquad \text{........................... (5)}$$

Function f in Eq. 5 represents the right-hand side of Eq. 4. After every time step enthalpy is converted to temperature with the help of enthalpy temperature relationship. Fourth order Runge-Kutta method discretisation error is of the order 4, by which reasonable accuracy can be expected even the ordinary differential equation is discretised in time.

In three-dimensional control volume method, three different types of boundary elements can be seen namely corner elements, edge element and face elements. As the name suggests corner element is positioned at the corners of the model with one eighth control volume. Similarly, edge element will be at the edges of the model with one fourth control volume and face element at the faces with half control volume as shown in Fig. 8.
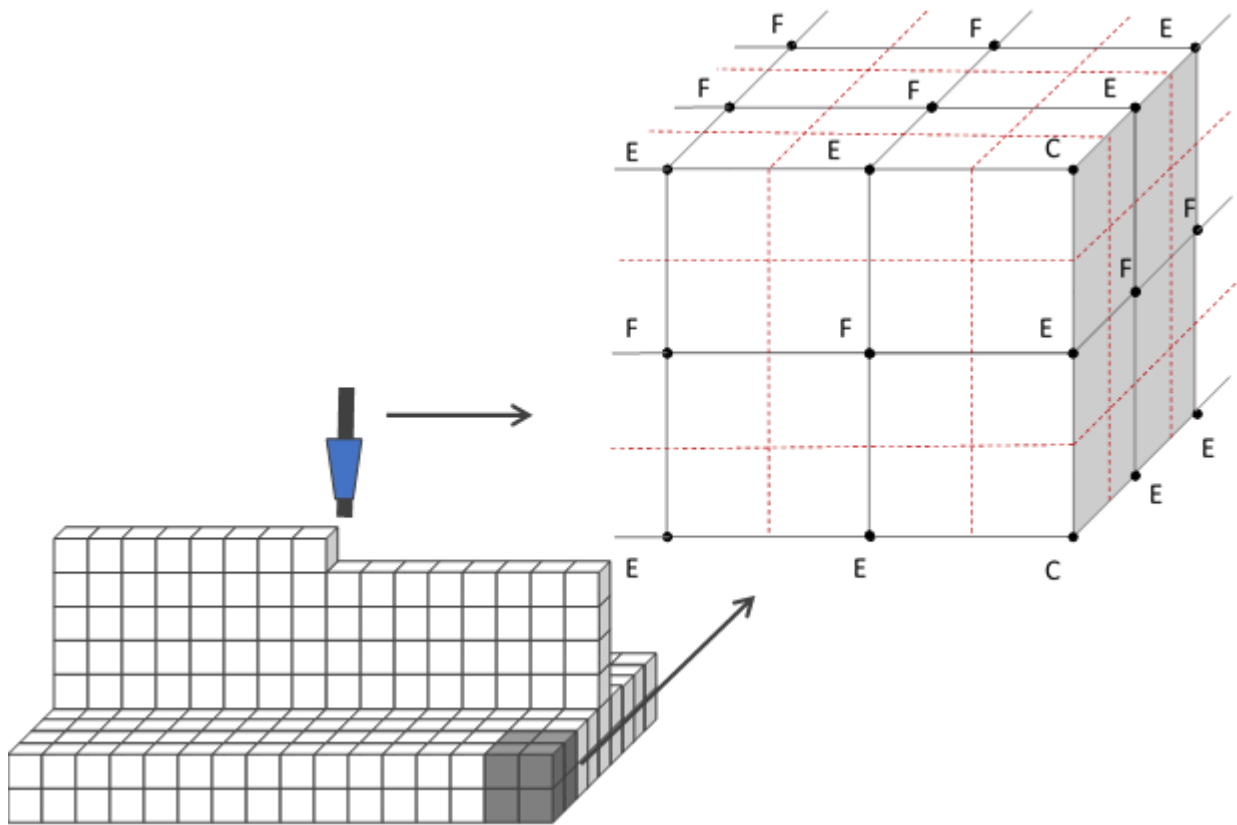
Fig.8 Representation of corner elements(C), edge elements(E) and face elements(F). Dashed lines represent element boundaries and solid lines joining the nodes

Average current and voltage is used to calculate the heat generated during arcing. Heat generation rate per unit volume due to arcing is given by Eq. 6,

$$Q_g = \frac{\eta\, V\, I}{\text{volume of element}} \ \text{J/mm}^3\, s \qquad\qquad \text{...................... (6)}$$

where,

η – arc efficiency,

V – voltage,

I – current.

A portion of the heat generated due to arcing are utilised to melt the electrode metal in GMAW and other portion reaches to the baseplate or the substrate on which bead is going to deposit. So, by considering the penetration some amount of heat is given to the element below the current activating element while the remaining portion is utilised for new element.

23

3.1.2 Meshing scheme

Single pass and 60 layers are modelled to simulate the deposition process. The mesh sizes used in the modelling are 2.5 × 2.5 × 2.5 mm. In this model, inactive element technique is implemented where in only active elements are included in the analysis which will reduce long number of computational runs. Initially all nodes of baseplate are assigned with room temperature i.e., 27 °C and the thermal properties are also assigned accordingly. The elements of beads are kept inactive until the heat source reaches the elements, once heat source passes from the elements, then they are considered to be active and will be involved in the analysis throughout. The time step is calculated on the basis of arcing frequency.

To have accurate prediction fine mesh is required but the model becomes computationally expensive due to increased number of nodes. Dynamic meshing strategy is introduced where two different mesh sizes are used to reduce the number of nodes. In this strategy, the mesh will be finer around the heat source as shown in Fig .9 where high temperature gradients are present. So, the finer mesh will be moved along with the heat source. This strategy helps in predicting the peak temperatures of thermal history accurately.
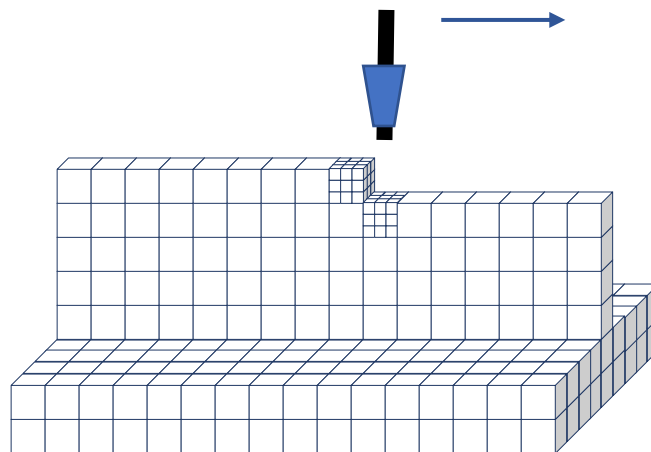

Fig.9 Dynamic meshing model

The number of nodes are less compared with complete finer mesh due dynamic meshing strategy which shows positive effect on computational efficiency less affecting the accuracy. But, the dynamic meshing predicts the peak temperatures of the thermal profiles accurately as the fine meshing is considered only in regions of heat source. The importance of current study lies in predicting cooling time from the thermal model. There is not much difference

observed in cooling times among coarse mesh and dynamic mesh models. So, coarser mesh size is considered throughout the model.

3.1.4 Time marching

Time step is controlled by Fourier number in order to achieve numerical stability. Critical time step can be given by Eq. 7.

$$\Delta t_{crit} \leq \frac{\Delta Z^2 \, Fo}{\alpha}$$ .... (7)

The displacement of the heat source in each time step is given by Eq. 8.

$$\Delta Z_{crit} = v \times \Delta t_{crit}$$ .... (8)

Where

Δz is the mesh size,

α is the thermal diffusivity and

Fo is the Fourier number.

It is understood from R.L. Ule et al [51] that the maximum allowable Fourier number is 0.37 and when Fourier number 0.22 the model rapidly losses numerical stability. It is found that the present model is more stable numerically at Fourier number 0.25. The motion of the heat source which is modelled according to the critical time step should be matched with the actual speed. So, the displacement of the heat source is compared with the element size to understand the number of elements need to be activated for each time step so as to match the speed of heat source modelled with actual. Three cases are possible by which decision can be made over activation of elements.

Case 1: $\Delta Z_{crit} < \Delta Z$

The displacement of the heat source for each time step is less than the element size in welding direction which means heat source remains in each element for a certain number of time steps which is given by,

$$n = \frac{\Delta Z}{\Delta Z_{crit}}$$

so, for n number of time steps heat source stays in each element. Figure 10 represents the jumping of heat source. For example, if the value of n is greater 1 which intimates that even for the next time step the heat source lies in the same element as ΔZ_{crit} is less than the mesh size or element size. Theoretically the

25

position of the source may be changed inside the element but the analytically this displacement does not show any affect because the heat source considered to be positioned at the same nodes.
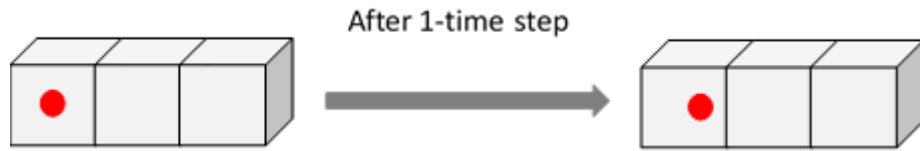

Fig.10 Heat source jump in one step for $\Delta Z_{crit} < \Delta Z$ case

Case 2: $\Delta Z_{crit} > \Delta Z$

The displacement of the heat source for each time step is greater than the element size in welding direction which means heat source jumps/activates certain number of elements in each time step. To have control on the number of elements activated in each time step, displacement of the heat source should be controlled which can be done as follows.

Assuming total number of jumps a heat source need to activate all elements in a bead as I_1 and constraining I_1 with $\Delta Z_{crit}' \leq \Delta Z_{crit}$.

where,

$$\Delta Z_{crit}' = \text{Pass length} / I_1 \qquad \text{.......................... (9)}$$

Here, $\Delta Z_{crit}'$ is required displacement of heat source in each time step. So, by incorporating $\Delta Z_{crit}'$ the number of elements activating in each time step can be controlled.

So, number of elements a heat source crosses in each jump are

$$I_2 = \Delta Z_{crit}' / \Delta Z \qquad \text{......................... (10)}$$

From the equations (7), (9) and (10), number of elements crossed in each jump by heat source controlling the total number of jumps, I_2 is given by,

$$I_2 = \sqrt{\frac{Fo \times \text{pass length} \times \text{weld speed}}{I_1 \times \alpha}} \qquad \text{.......................... (11)}$$

From above equation, I_2 can be found directly for any assumed I_1 satisfying the Eq.8.

26

So, the number of the elements that are activated in each time step can be calculated from Eq. 11. For instance, I_2 is two, which means the heat source is controlled to cover only two elements in each time step. So, in every time step two element are activated. Figure 11 represents the position after finishing one-time step however the second and the third elements are activated.
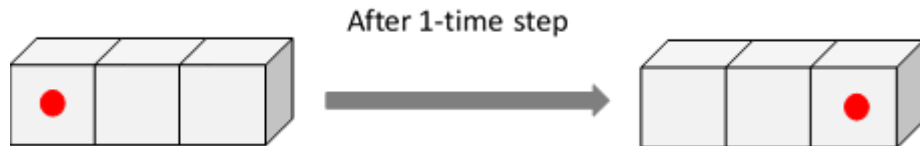

Fig.11 Heat source jump in one step for $\Delta Z_{crit} < \Delta Z$ case

Case 3: $\Delta Z_{crit} = \Delta Z$

The displacement of the heat source in each time step is equal to the element size in welding direction which means heat source jumps exactly one element in one-time step. This indicates for one-time step one element is going to be activated. In this case as the both critical distance and the mesh sizes are same, it is understood that the new position of heat source will be in next element after finishing one-time step which is shown in Fig. 12.
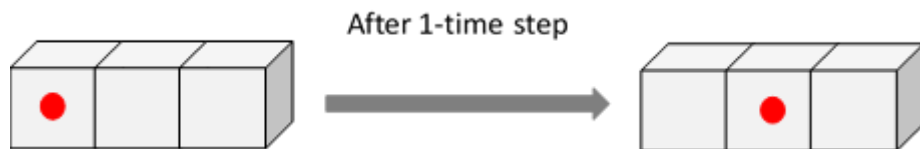

Fig.12 Heat source jump in one step for $\Delta Z_{crit} = \Delta Z$ case

In this way marching of the heat source is controlled with the help of Fourier number in the current model. The current model can analyse multi-pass multi-layer scenario and flexible enough to understand the effects of various process parameters on thermal aspect of the component. Provision is given to choose any allowable combinations among interpass temperature, interpass time, interlayer temperature and interlayer time. These parameters can be defined as follows.

New pass is deposited only after the previously deposited pass cools down to certain temperature known as interpass temperature. New pass is laid only after certain waiting time known to be interpass time. Similarly, New layer is deposited only after the previously deposited layer cools down to certain temperature known as interlayer temperature and new layer is laid only after certain waiting time known to be interlayer time. The approach of the thermal model is shown clearly in the flow chart shown in Fig. 13 and Fig. 14. This thermal model is integrated with the hardness model to predict the hardness variation in the component. The hardness model is discussed in the following sub section.

3.1.5 Temperature dependent thermophysical properties

For low carbon steel following relations are considered to calculate temperature dependent thermophysical properties

Thermal conductivity (W/m °C)	$53 - 0.04$ (T-27)	$27 \leq T$ (° C) ≤ 727
	$25 + 6.25 \times 10^{-3}$ (T - 727)	$727 \leq T$ (° C) ≤ 1527
	125	T (° C) ≥ 1527

Enthalpy per unit volume (J/m^3)	4.23×10^6 (T)	$0 \leq T$ (° C) < 650
	$2.75 \times 10^9 + 2 \times 10^7$ (T - 650)	$650 \leq T$ (° C) < 675
	$3.25 \times 10^9 + 5.48 \times 10^7$ (T - 675)	$675 \leq T$ (° C) < 1450
	$7.5 \times 10^9 + 5.5 \times 10^7$ (T - 1450)	$1450 \leq T$ (° C) < 1500
	$10.25 \times 10^9 + 4.5 \times 10^6$ (T - 1500)	T (° C) ≥ 1500

Figure 13 represents the temperature dependency of thermal conductivity plot. Till 1527 °C variation with temperature is considered after which it is considered to be constant. [50]
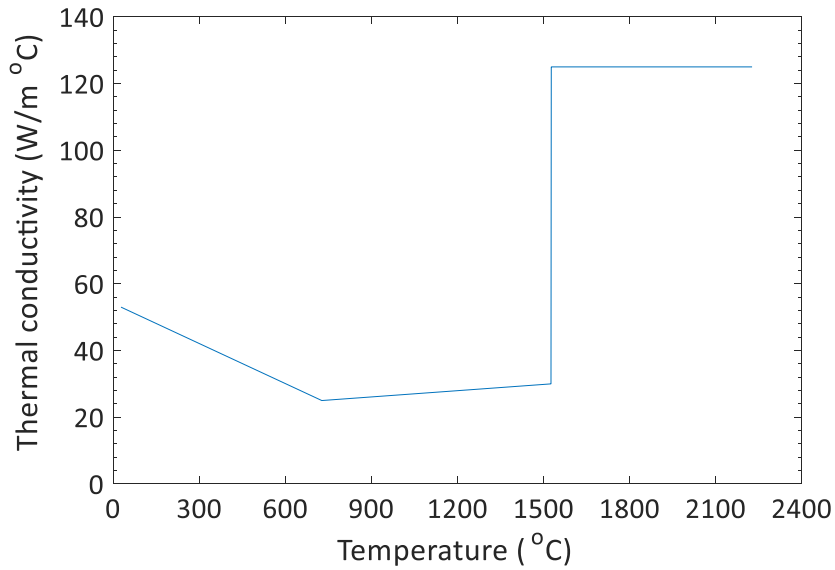
Fig.13 Thermal conductivity variation with temperature [50].

3.1.6 Assumptions

- Convective and radiative losses from the element are neglected while arcing.
- Bottom surface of the baseplate is maintained at room temperature all the time so as to accommodate heat losses to fixture.
- Combined convective and radiative heat transfer coefficient is considered as

$$h = 24.1 \times 10^{-4} \; \varepsilon \; T^{1.61}$$
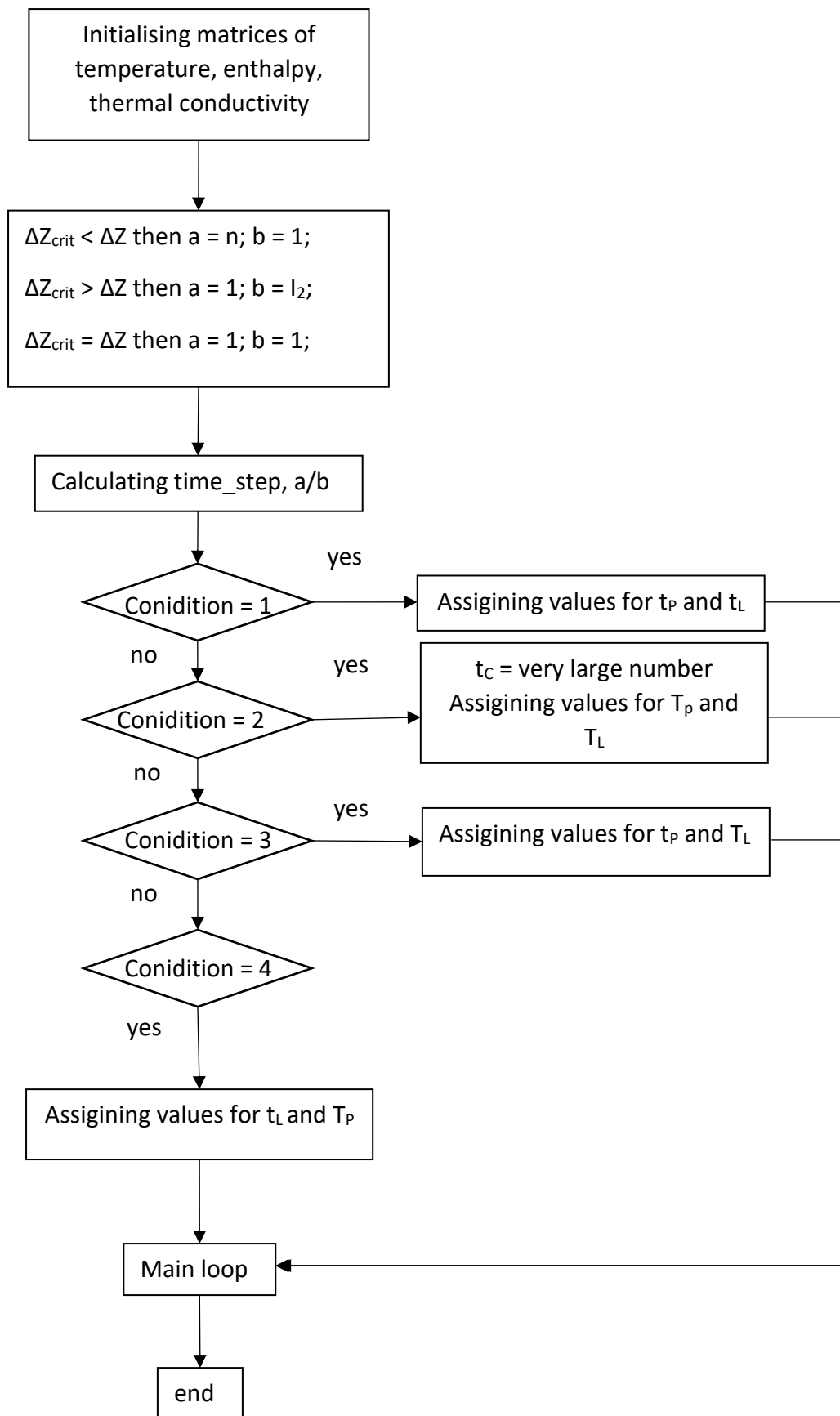
where, ε (emissivity) – 0.82

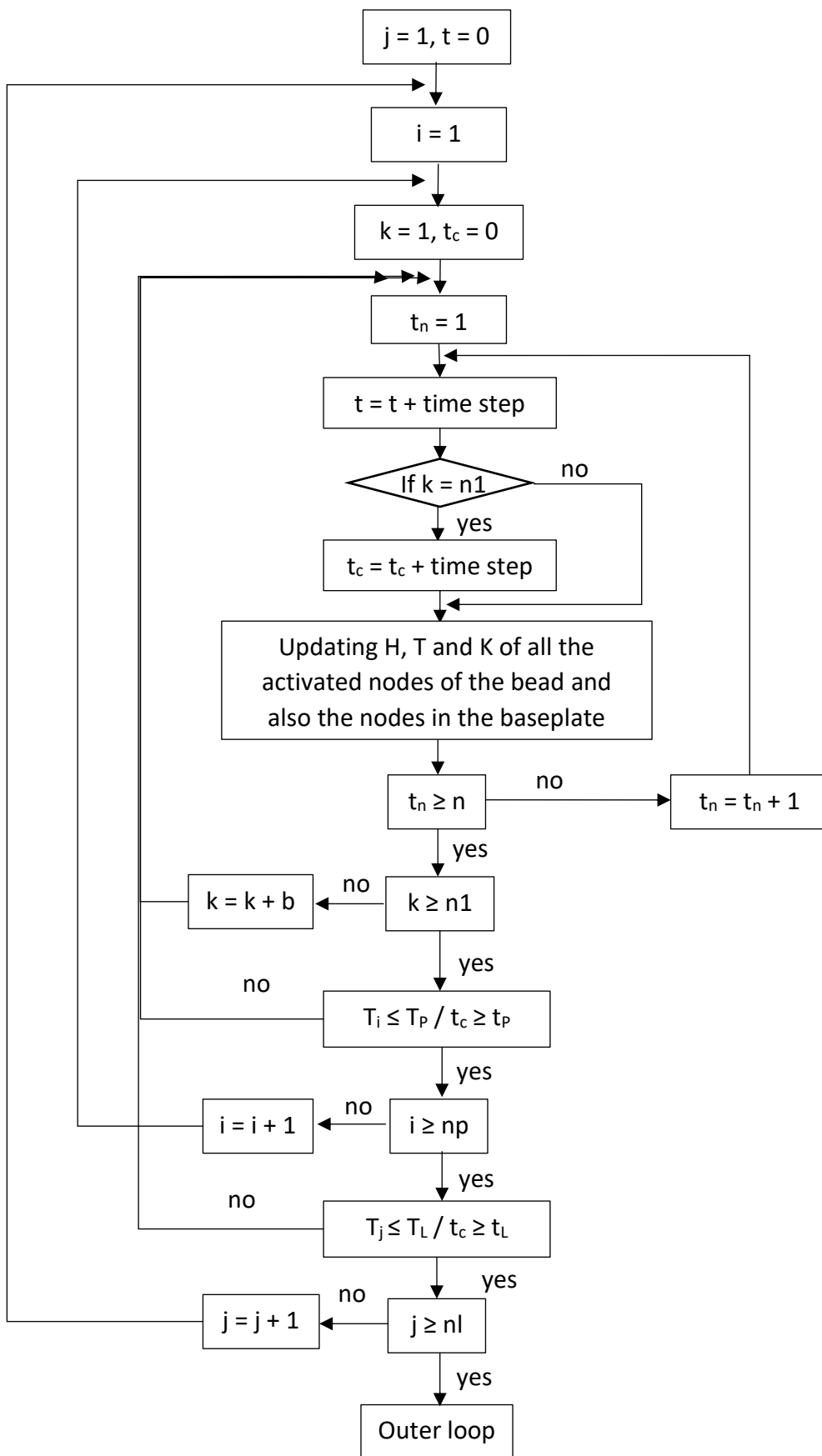Fig.14 Flow chart describing thermal modelling procedure

Fig.15 Flow chart of thermal modelling main loop

Variables used in the flow chart,

T_P – interpass temperature

T_L – interlayer temperature

t_P – interpass time

t_L – interlayer time

n – number of time steps heat source stays in each element

n1 – number nodes along the deposited direction

nl, np – total number of layers and passes respectively

T_i – temperature of middle element in the ith bead

T_j – temperature of middle element of middle pass in j^{th} layer

t, t_C – time and cooling time respectively

j, i – takes values from 1 to nl, np respectively

k – takes values from 1 to number of nodes in a bead along the depositing direction

t_n – takes values from 1 to n

Table.3 Input data used in computation in thermal model.

Voltage, V	11.6 volts
Current, I	85 amps
Arc efficiency, η	0.75
Welding torch speed, v	400 mm/min
Density of steel, ρ	7854 kg/m^3
Specific heat of steel, C_p	509.3 J/kg K
Inter layer temperature, T_{inL}	93 °C
Surface emissivity, ε	0.82
Room temperature, T_{room}	27 °C
Penetration	1.2 mm

3.2 Hardness model

Empirical formulas to calculate hardness with independent variables as percentage mass concentrations of the elements, austenitizing temperature and the cooling rate is proposed by Trzaska [54] for the steels cooled from austenitic temperature is integrated with the present thermal model. Multiple regression and logistic regression methods are used to develop the following empirical relations.

General hardness model,

$$HV = 3.7 + 225 \cdot C + 82 \cdot Mn + 28 \cdot Si + 55 \cdot Cr + 28 \cdot Ni + 53.5 \cdot Mo + 147 \cdot V + 71 \cdot Cu + 0.09 \cdot T_A - 3.8 \cdot \sqrt[4]{V_c} + 68 \cdot C \cdot \sqrt[4]{V_c} - 42 \cdot W_f - 69 \cdot W_p - 32.5 \cdot W_b + 72 \cdot W_m$$

……………………… (12)

Hardness model for martensitic structure,

$$HV_m = 200 + 824 \cdot C + 44 \cdot Mn + 14 \cdot Cr + 9 \cdot Ni + 171 \cdot V + 78.5 \cdot Cu + 4.13 \cdot \sqrt[4]{V_c}$$

……………………… (13)

Hardness model for ferrite-pearlite structure,

$$HV_{f-p} = -73 + 253 \cdot C + 52 \cdot Mn + 10 \cdot Si + 36 \cdot Cr + 8 \cdot Ni + 20 \cdot Mo + 80 \cdot V + 0.11 \cdot T_A + 12.5 \cdot \sqrt[4]{V_c}$$

……………………… (14)

where,

W_x is dichotomous variable

x – f(ferrite), p(pearlite), b(bainite), m(martensite)

C, Mn, Si, Cr, Ni, Mo and V are the percentage mass fractions of respective elements

T_A is Austenitizing temperature

V_c is cooling rate

HV_m and HV_{f-p} can be used only after proper classification results are obtained.

$$W_x = \left\{ \begin{array}{l} 0 \text{ if } S_x \leq N \\ 1 \text{ if } S_x > N \end{array} \right\}$$

W_x describes the occurrence of various microstructure on the basis of another variable S_x. W_x takes the value '0' when the variable S_x is less than or equals to the threshold value (N), which

represents the non-occurrence of respective microstructure while W_x as '1' represents the occurrence.

$$S_x = \frac{\exp(k_x)}{1 + \exp(k_x)}$$

where,

N = 0.5 for ferritic, pearlite and martensitic transformation

N = 0.4 for bainitic transformation

$$k_f = 18.4 - 15.4 \cdot C - 1.9 \cdot Mn + 0.7 \cdot Si - 2.5 \cdot Cr - 1.5 \cdot Ni - 4.8 \cdot Mo + 2.4 \cdot V + 1.4 \cdot Cu - 0.004 \cdot T_A - \sqrt[4]{V_c}$$

$$k_p = 12 - 1.4 \cdot C - 2.3 \cdot Mn - 2.3 \cdot Cr - 1.4 \cdot Ni - 6 \cdot Mo + 3.9 \cdot V - 0.002 \cdot T_A - 1.2 \cdot \sqrt[4]{V_c}$$

$$k_b = 1.3 - 3.7 \cdot C + 0.45 \cdot Mn + 0.2 \cdot Cr + 0.18 \cdot Ni + 1.9 \cdot Mo - 0.17 \cdot \sqrt[4]{V_c} - 0.57 \cdot \sqrt{(4.35 - \sqrt[4]{V_c})^2}$$

$$k_m = -16.5 + 4.7 \cdot C + 2.6 \cdot Mn + 0.6 \cdot Si + 2.4 \cdot Cr + 1.2 \cdot Ni + 1.9 \cdot Mo + 4.8 \cdot Cu + 0.006 \cdot T_A + 1.1 \cdot \sqrt[4]{V_c}$$

The limiting range of the mass concentrations of elements for which above equations are applicable is as shown in Table. 4. Other conditions that limits the applicability of the model is shown in Table. 5.

Table.4 Critical range of compositions for hardness model

	Mass fractions of elements, %							
	C	Mn	Si	Cr	Ni	Mo	V	Cu
Min	0.06	0.13	0.12	0	0	0	0	0
Max	0.68	2.04	1.75	2.3	3.85	1.05	0.38	0.38

Table.5 Critical range of combinations of compositions for hardness model

	Mass fractions of elements, %			
	Mn+Cr	Mn+Cr+Ni	Cr+Ni	Mn+Ni
Maximum	3.6	5.6	5.3	4.5

This hardness model is combined with the thermal model to predict the hardness of the component.

3.3 Overview of the Integrated model

The overview of this integrated model is as shown in Fig. 16. Various input parameters are required for thermal model which means effect of those parameters on the thermal data and hardness can be understood from this tool. From the figure, it can be seen that one of the inputs of hardness model is calculated from the thermal model
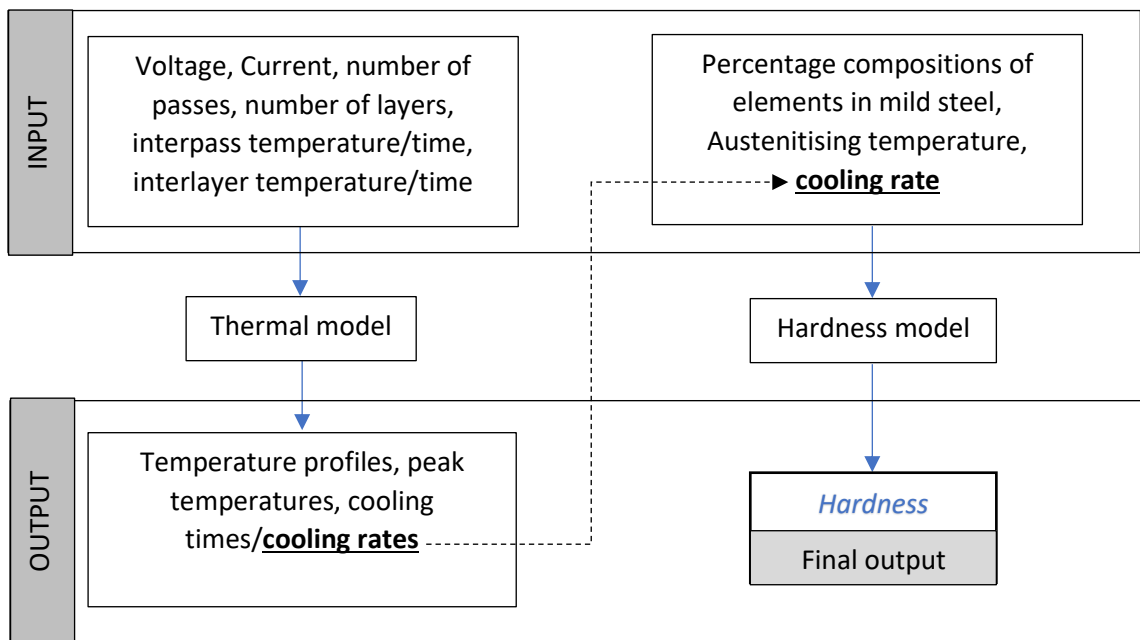

Fig.16 Overview of Integrated thermal and hardness model

Chapter 4

Experimental details

Overview

The brief explanation of the machine setup used and the deposition techniques performed is discussed in this chapter. Information of the various parameters and the materials used are presented. Finally, the mounting method for polishing the samples and the instruments used to investigate microstructure and hardness are briefed here.

4.1 Methodology and Investigations

Cold metal transfer (CMT) weld deposition technique is used to deposit the metal over the substrate. The welding torch is mounted on the computer numerical control (CNC) vertical milling machining centre to achieve controlled positioning and motions. Mild steel is used as the substrate with dimensions of 300 mm X 150 mm X 25 mm. Filler wire, ER70S-6 of 0.8 mm diameter is used. Metal is deposited at a speed of 400 mm/min with arcing frequency as 50 Hz and the shielding gas mixture is maintained at the ratio 82:18 of CO_2 and Ar.
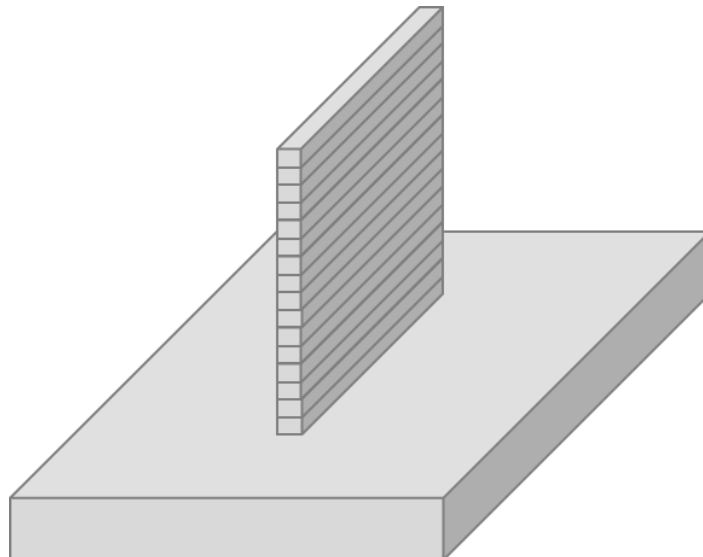

Fig.17 Representative model of the manufactured component

A thin walled component with the dimensions of 180 x 120 x ~3.5 mm is manufactured. 60 layers are deposited one over the other, reaching the height of around 120 mm. Every new layer is deposited only when the surface temperature of the last deposited layer reaches 93°C known as interlayer temperature. The layers are deposited in the middle of the substrate and every alternate layer deposited in the direction opposite to previous one as shown in Fig. 17. Samples are cut along the built-up direction from the central portion of the component. As the samples are long enough it is difficult to use hot or cold mounting methods. So, polishing is done by fixing the samples to a mounting plate with the help of thermoplastic moulding material as shown Fig. 18.

Fig.18 Samples fixed on a mounting plate for polishing

Samples are polished using different grit sizes namely 400, 600, 800, 1000, 1200 followed by diamond polishing of 3 μm, 2 μm and 1μm size particles. Nital, 95% ethanol and 5% nitric acid is used as etchant. Microstructures are observed at various regions of the samples under Field Emission Scanning Electron Microscope (FESEM). Hardness values are measured with Vickers Hardness Testing machine at a load of 1 Kgf along the built-up direction.

Chapter 5

Results and Discussions

Overview

In this section, the experimental investigations of microstructure and the hardness variation along the built-up direction are discussed. Then the predicted thermal cycles and cooling time are investigated and the comparison of experimental hardness with predicted one is made. Lastly, the effect of pre-heating the base plate and an approach to achieve uniform properties are discussed.

5.1 Experimental Outcomes

5.1.1 Microstructures and Hardness measurement

The microstructures are taken at different locations along the built-up directions namely top, above mid, mid, below mid and the bottom regions. From Fig. 19, it can be observed that the grain size is finer in bottom region, coarser grain size in the middle region and the medium grain size is in the top region. It is believed that the portion of the component which is in the thermal vicinity of the baseplate undergone comparatively high cooling rate resulting in finer grain size even though there is chance of grain growth due to repeated heating and cooling cycles.
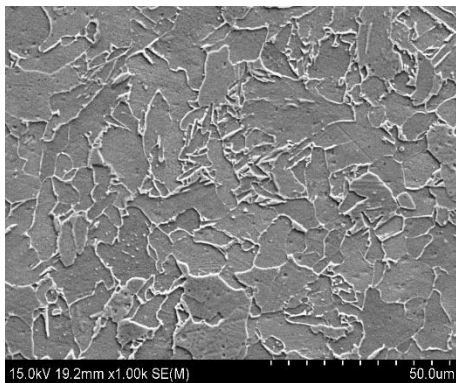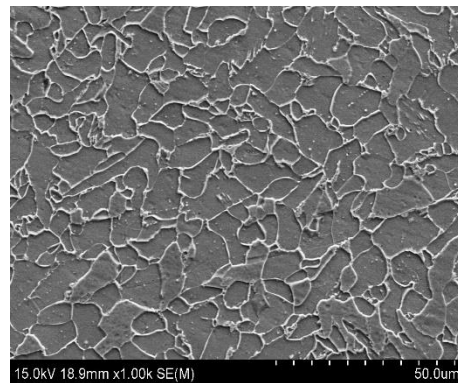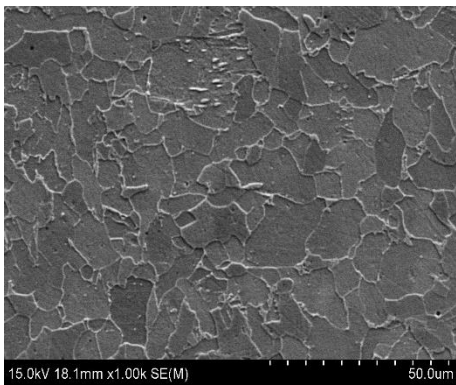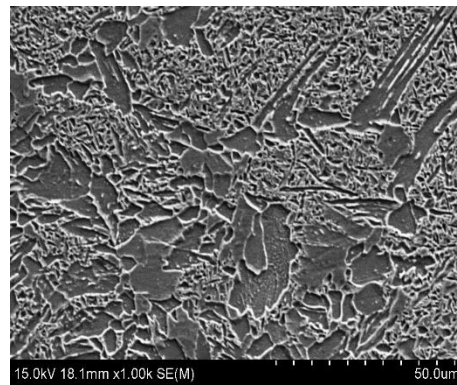

top	above mid
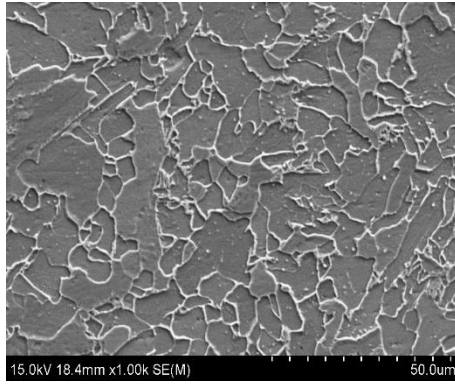
Mid

Below mid

bottom

Fig. 19 Microstructures of naturally cooled component taken near the outer edge

The coarser grain size in remaining portion of the component except top few layers, because of grain growth due to repeated heating and cooling. The top few layers undergo slightly higher cooling rate compared to the middle region but lesser compared to the portion near the baseplate resulting in medium grain size. Mostly the mixture of Pearlite and Ferrite phases are observed throughout the component with different grain sizes and structures.

The hardness measurement is carried out along the built-up direction of the component. This variation of hardness in the component shown in Fig. 20 is because of thermal cycles and the baseplate. All the thermal cycles through which each layer undergoes does not affect the microstructure and the grain size. The number of cycles that shows effect on the layer is named as effective thermal cycles. The variation of hardness is observed in the regions near the baseplate which may be because of high cooling rate and in the top layers due to difference in number of effective thermal cycles they undergone. The remaining portion exhibits uniform hardness due to uniform cooling rate. The layers that are not in thermal

39

vicinity of the baseplate and undergone through same effective thermal cycles are believed to have uniform cooling rate.
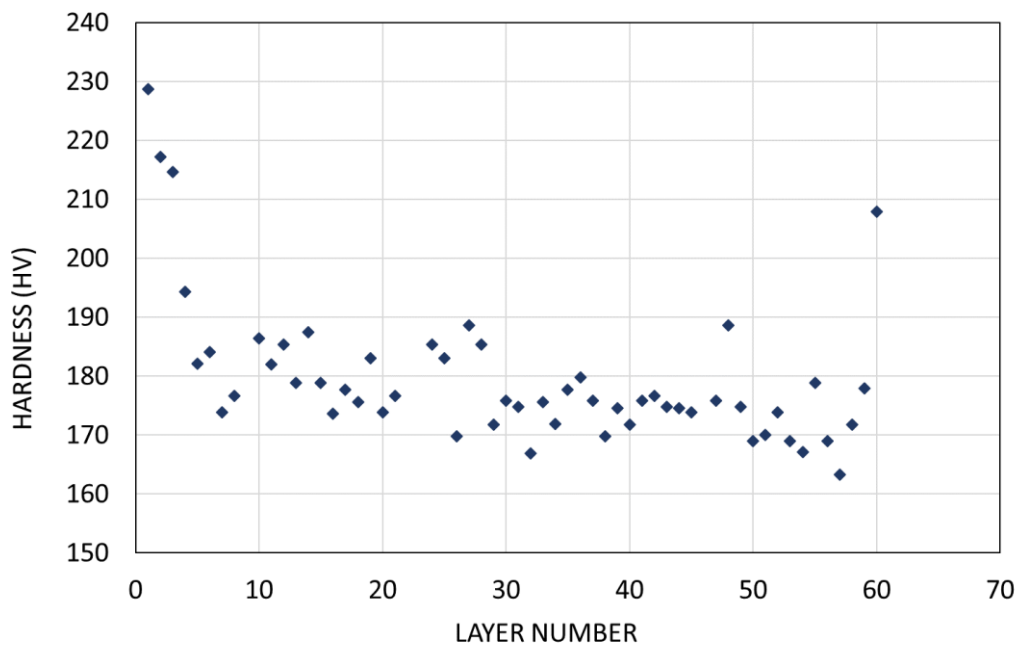

Fig.20 Variation of experimentally measured hardness along built-up direction for natural case

Reasons behind the property variation is discussed above and the predicted hardness plots from the integrated model is discussed in the following section.

5.2 Model Outcomes

5.2.1 Prediction of thermal cycles, cooling times and hardness

The thermal history for single pass sixty layers are generated. Figure 21 shows the temperature profiles for middle element of the twentieth layer and fortieth layer respectively are used to illustrate the thermal process that component undergone through. It is observed that when heat source passes through the element, peak temperature of it reaches to 1950 °C and the subsequent peaks of the element are formed when heat source passes through the elements above to it. The gradually reduced peaks that are observed in thermal profiles is due to increase in distance between the heat source and the element. From Fig. 21 it can

be observed that the effect of new layer deposition is almost negligible on the layers that are 20 layers away from the current depositing one.
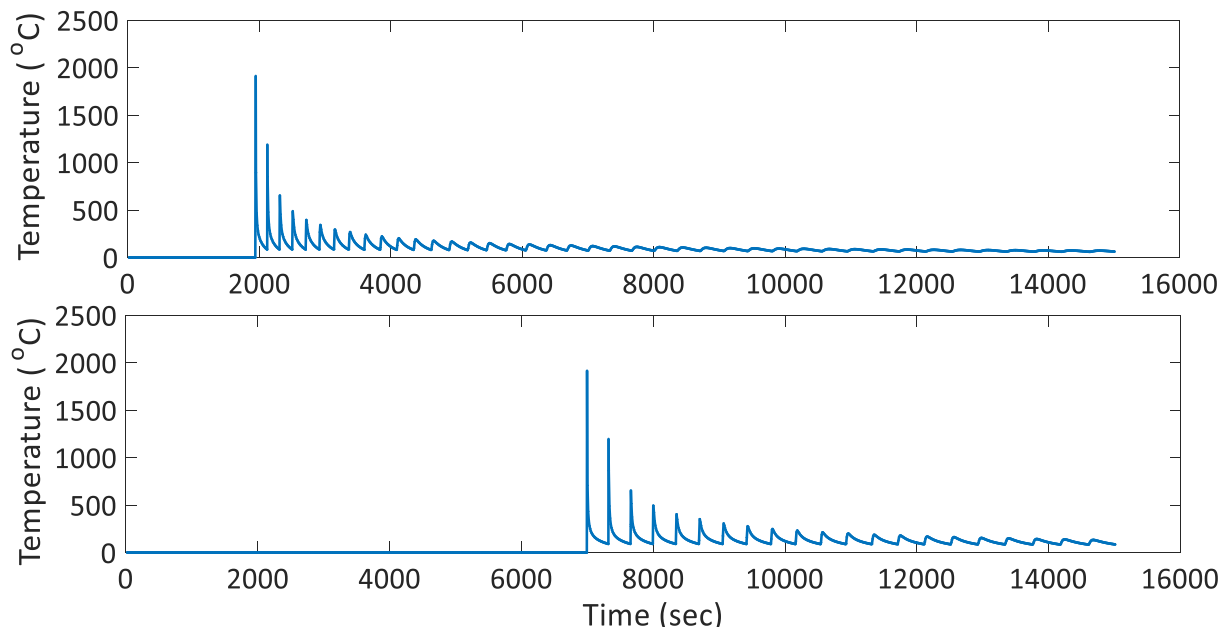

Fig. 21 Thermal cycles of middle elements of the twentieth layer and fortieth layer

For mild steel, region of interest is from 800 °C to 500 °C because most of the microstructural changes takes place here itself. This is the region where the solid-state transformation of austenite occurs. From the Fig. 21, it is understood that the peak temperatures of the layer reach 800 °C i.e., austenitic temperature, only for the deposition of the next few layers. It can also be realised that the number of peaks reaching austenitic temperature becomes less for the last few layers. So, number of times any element of the component reaching austenitic temperature is same for all the layers except for the last few. The time taken to cool from 800 °C to 500 °C is $T_{8/5}$ time. In this model, cooling rate of desired element is calculated with $T_{8/5}$ time from the last peak that crosses 800 °C in thermal cycle because it is believed that microstructural changes occur lastly due to the peak that crossed austenitic temperature zone lastly. Figure 22 shows the $T_{8/5}$ time of the middle elements of all 60 layers which are calculated at the last peak of the thermal cycle that crossed austenitic temperature zone. From Fig. 22, it can be observed that cooling time increases gradually till 10th layer after which it is almost uniform except for last few layers. For the last few layers the number of thermal cycles that are undergone decreased gradually which results in variation in cooling time.
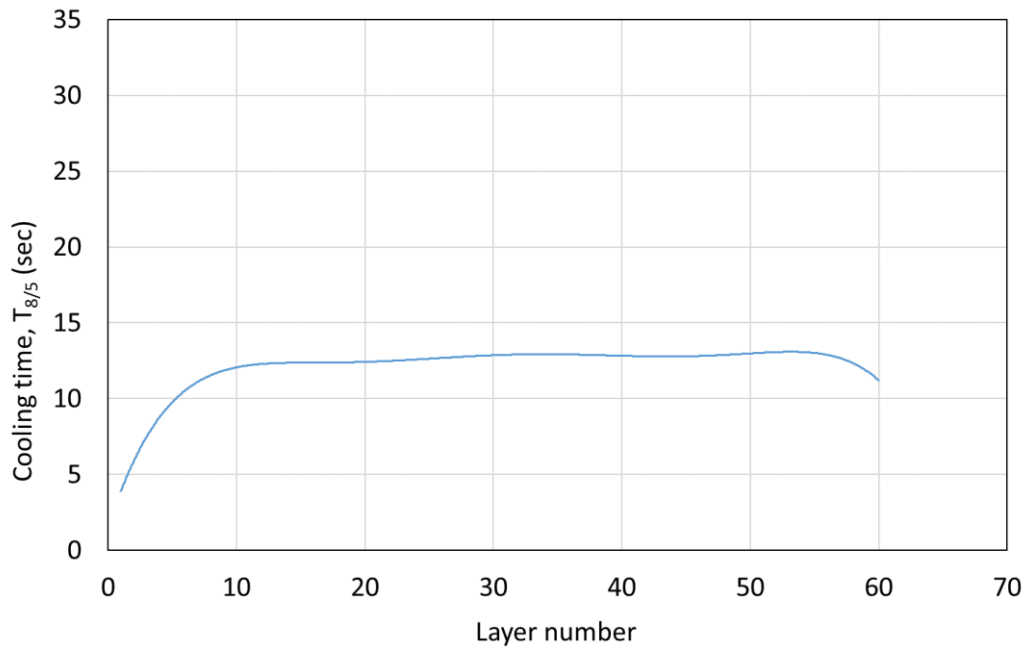
41

Fig.22 Variation of cooling time of last effective peak with the layers

From the microstructures, with conformation of pearlite and ferritic phases it is understood that hardness can be predicted with the help of HV_{fp} Eq. 14. Cooling rate of all the layers is calculated from $T_{8/5}$ time. Hardness is predicted along the built-up direction and is in good agreement with experimental one as shown in Fig. 23. The hardness prediction from the thermal model can be used as a tool to understand the effects of strategies like controlling process parameters and other cooling rate controlling scheme on mechanical properties. With the help of this model, the effect of heating the baseplate before layers deposition on hardness is studied and an approach to achieve better uniform mechanical properties is proposed in the next sub section.
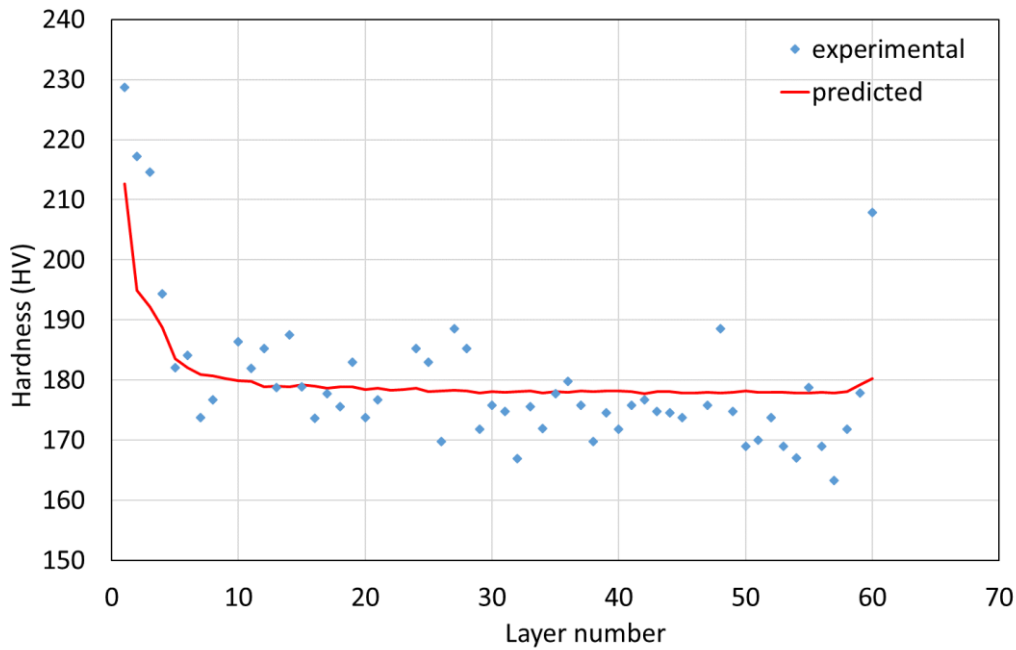
Fig. 23 Comparison between predicted hardness with experimental hardness along the built-up direction

5.2.2 Effect of preheating the baseplate on hardness

To understand the effect of preheating baseplate temperature over the hardness of the component, different cases are studied with the help of current model in which bottom surface of the baseplate is maintained at different temperatures like 27 ℃, 127 ℃, 227 ℃, 327 ℃ and 427 ℃ throughout the manufacturing process. Figure 24 shows the comparison of the above cases from which it is understood that with increase in baseplate temperature, hardness of the deposited layers that are in thermal vicinity of baseplate decreased due to decrease in cooling rate. The cooling rate is decreased due to decrease in thermal gradient with the baseplate. It is observed from Fig. 24 that the hardness value for the first layer with baseplate temperature 373 ℃ are almost same to that the case of 27 ℃ for layers above 10. Almost uniform properties are observed in the case of 427 ℃ but this case results in softer component. However, an understanding is developed from this study that the better uniform hardness can be achieved by depositing the layers over heated baseplate then by controlled cooling of baseplate for the subsequent deposition.
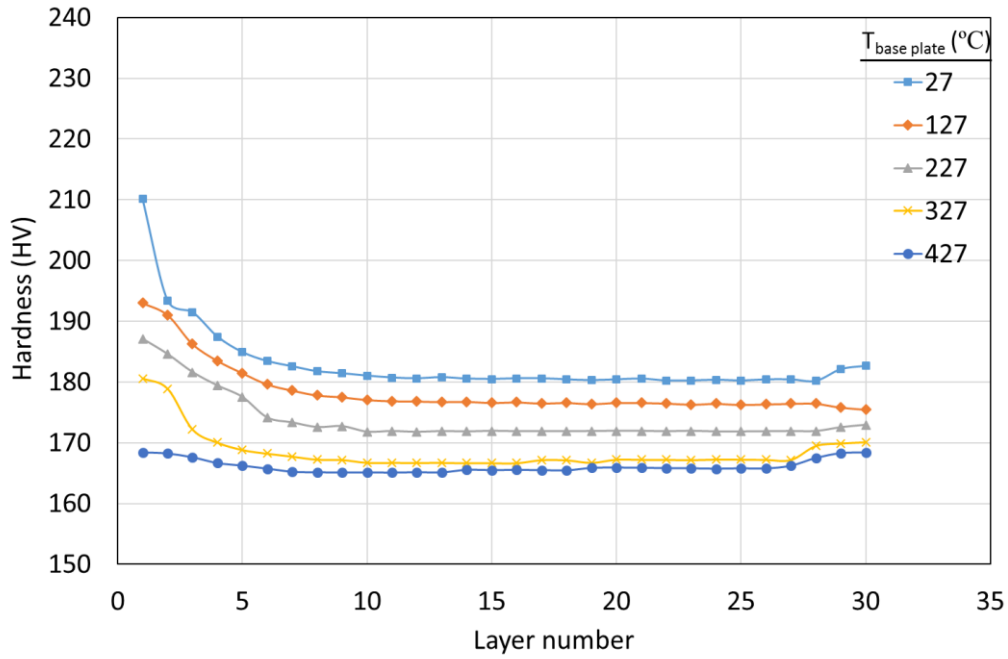
Fig.24 Effect of maintaining constant baseplate temperature throughout fabrication

5.2.3 Approach to achieve uniform hardness

The baseplate is heated to certain temperature($T_{initial}$) initially on which layers are to be deposited. Before deposition of new layer, it should be ensured that the baseplate temperature is cooled by ΔT temperature and process is repeated till temperature of the baseplate reaches to T_{final}. Once the bottom surface of baseplate reaches T_{final}, the temperature is maintained at T_{final} for the remaining depositions. For instance, the bottom surface of baseplate is maintained at $T_{initial}$ while the deposition of first layer, second layer is deposited only after ensuring the bottom surface temperature of baseplate reaches ($T_{initial}$ - ΔT), third layer is deposited only after ($T_{initial}$ - $2\Delta T$) and so on. The bottom surface temperature of the baseplate will be greater than T_{final} till the deposition of N number of layers which is given by,

$$N \approx \frac{T_{initial} - T_{final}}{\Delta T}$$

The minimum base plate temperature T_{final}, allowed is around preheat temperature i.e., 93 ℃ which ensures no cracking and distortions in the component. So, from Fig. 24 $T_{initial}$ can be expected to be in the range of 327 ℃ and 427 ℃ to achieve uniform hardness keeping T_{final}

as 93 ℃. Further, investigations are carried out to understand the effect of $T_{initial}$, ΔT and T_{final} over the hardness.

It can be observed from Fig. 25 that the $T_{8/5}$ time of the first layer is more when the bottom of the baseplate is initialised with 427 ℃ compared with other cases. After certain number of layers, the $T_{8/5}$ time is observed to be same for the 3 cases. The fluctuations for the curve of $T_{initial}$ 427 ℃ are more compared to other cases due to high N value. After N layers of deposition, as the temperature of bottom surface of baseplate is kept constant at T_{final}, $T_{8/5}$ time can be seen to be constant. Similarly, as T_{final} temperature is constant for these cases, $T_{8/5}$ time is constant for the layers after N.

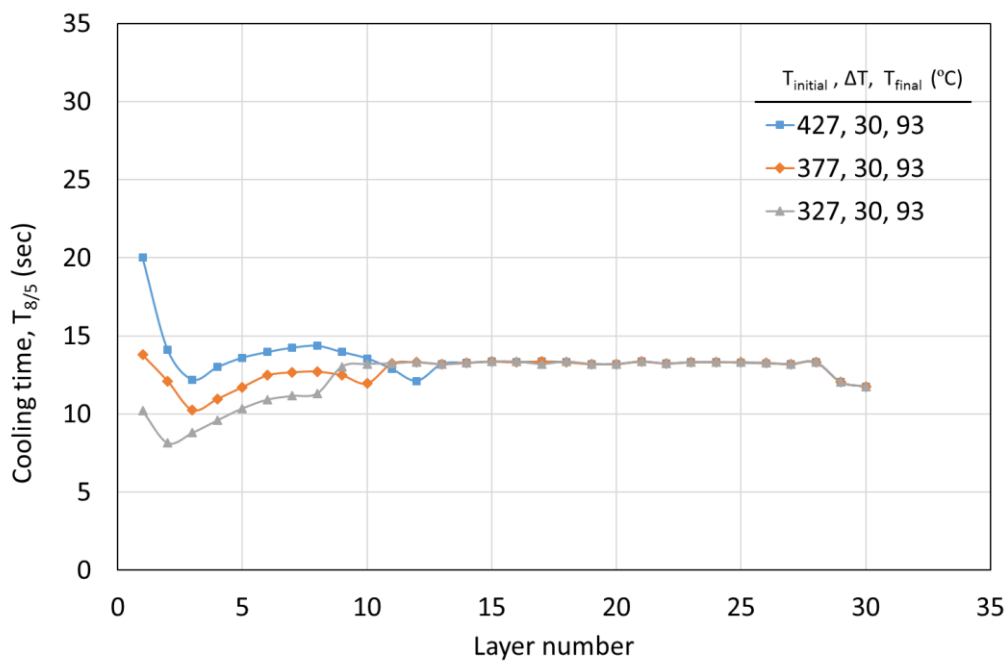Fig. 25 Effect of pre-heated baseplate temperature($T_{initial}$) over cooling time

From the Fig. 26, it can be seen that when $T_{initial}$ is 427 ℃ the layers which are in thermal vicinity of the baseplate have comparatively more cooling time became of which softer structure can be achieved and for $T_{initial}$ is 327 ℃ they became comparatively hard. $T_{initial}$ as 377 ℃ is the best one to achieve uniform properties.
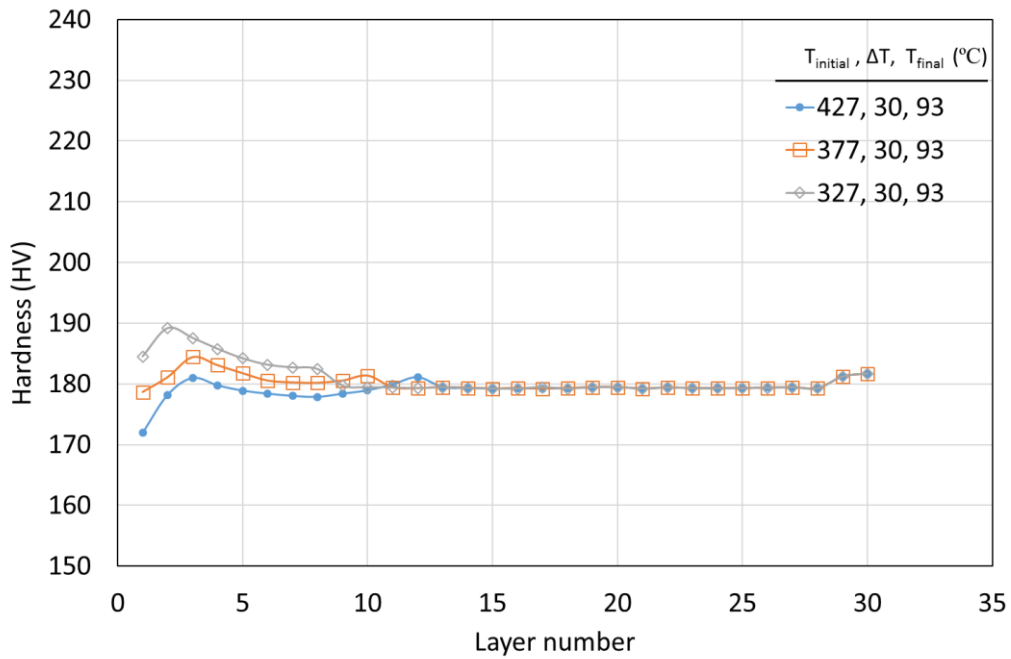
Fig. 26 Effect of pre-heated baseplate temperature($T_{initial}$) over hardness

Figure 27 shows the effect of ΔT on cooling time wherein it is observed that the magnitude of deviation is observed to be comparatively less in the case of 20. This gives an understanding that the better properties can be achieved with the case of 20.
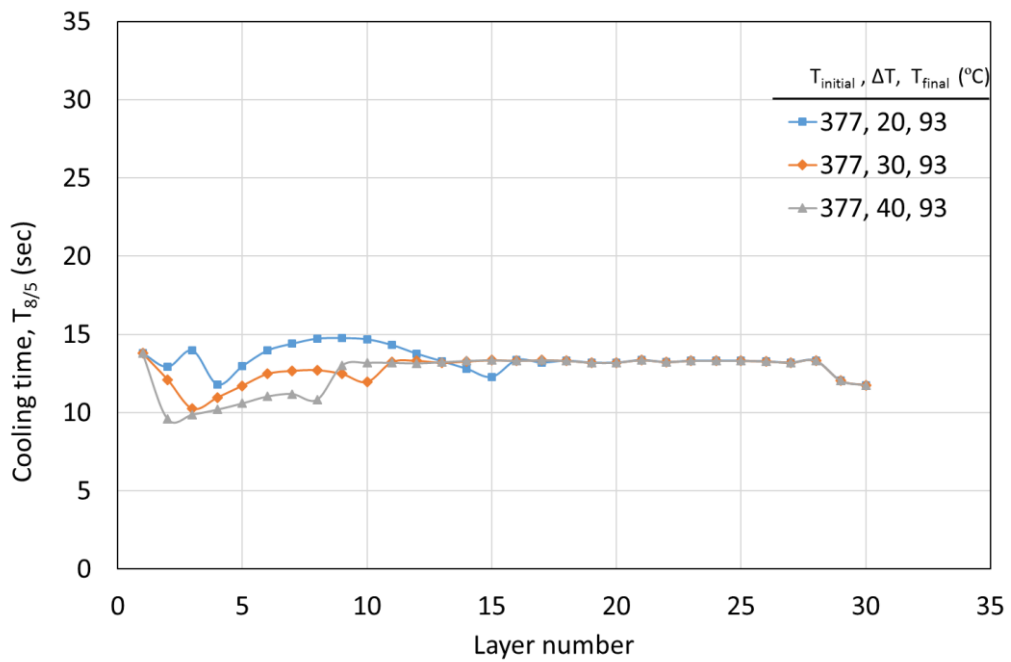
Fig. 27 Effect of ΔT over cooling time

The hardness values are predicted to be uniform in the case of 20 and these values are constant after respective N layers. From the Fig. 28, it can also be said that as ΔT decreases N value increases by which further more fluctuations may occur.
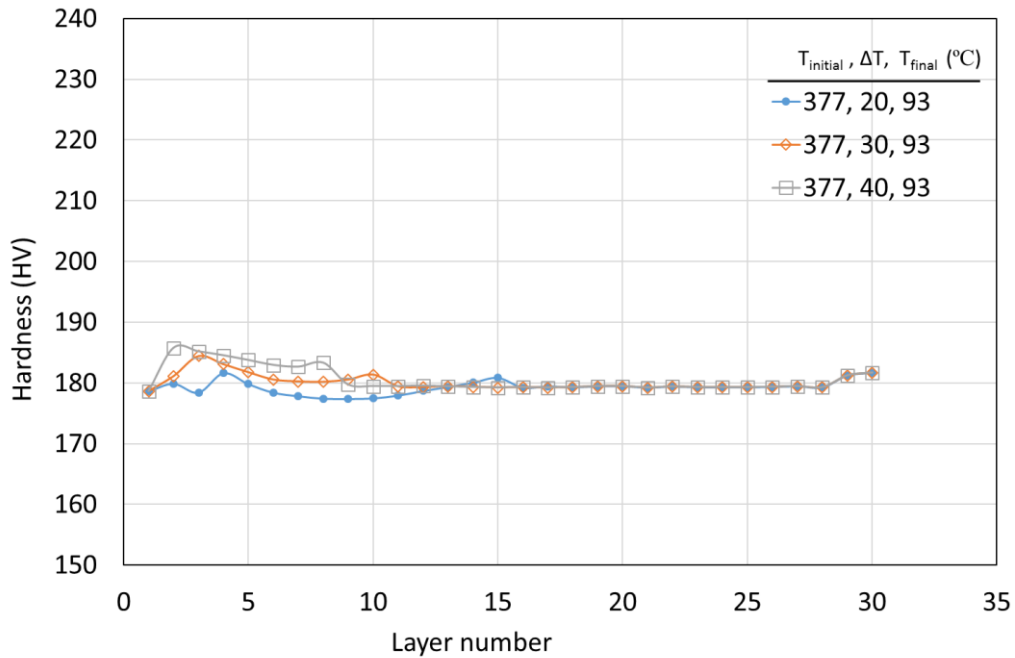
Fig. 28 Effect of ΔT over hardness

From Fig. 29, it can be understood that the effect of T_{final} temperature is observed after N layers. T final do not affect the first N layers. With increase of T_{final} cooling time also increases which can be observed in Fig. 30.

When T_{final} is less than pre heat temperature the layers after respective N became comparitively harder where as they became softer when the temperature is greater than preheat temperature as shown in Fig. 30. However, the T_{final} is better to maintain at preheat temperature to avoid cracks and distortions in the final component.

Fig. 29 Effect of T_{final} over cooling time

Fig.30 Effect of T_{final} over hardness

From the study of ΔT effect on hardness, it can be observed that the values are less deviated from the mean when the ΔT is less among the considered values. From the investigations

carried out for $T_{initial}$, the region to achieve best uniform hardness can be known, but to find the exact $T_{initial}$, further studies are needed.

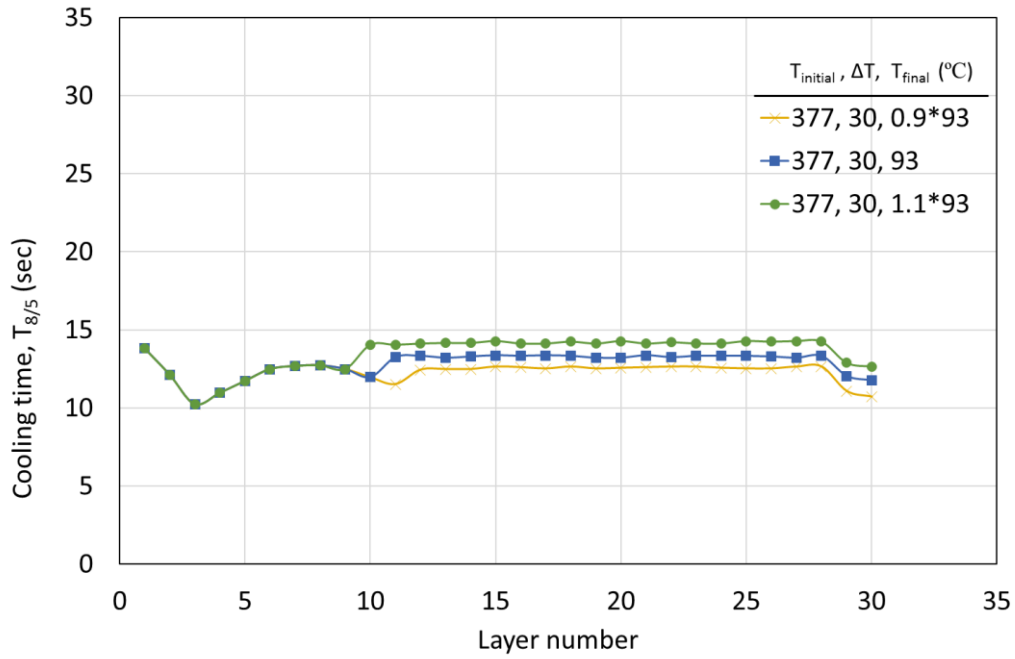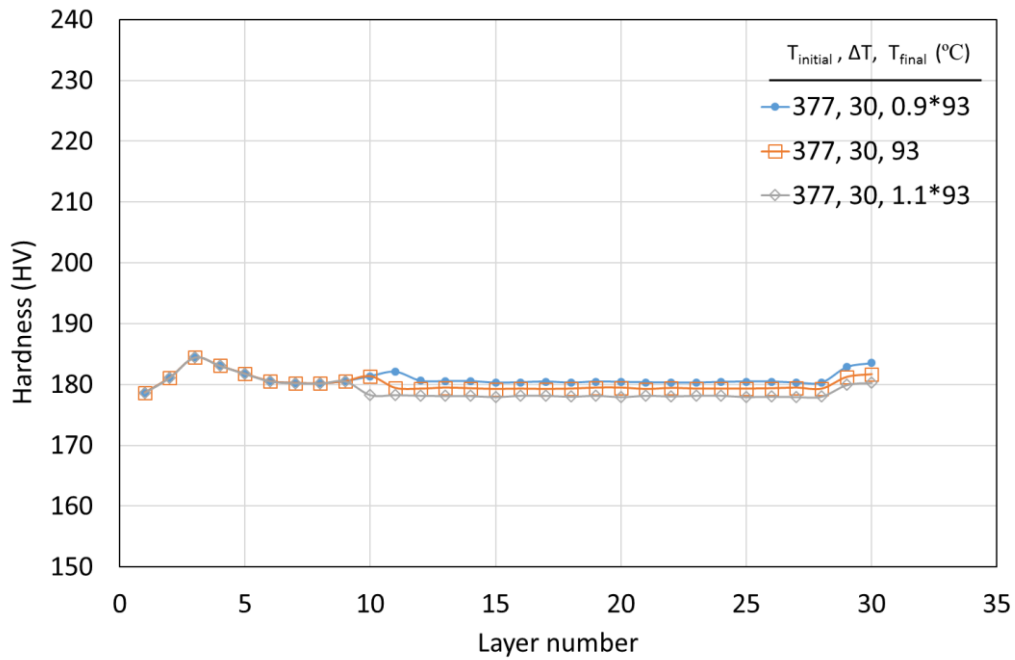Further simulations are carried out for single pass 30 layer at various combinations of $T_{initial}$ and ΔT that are in the best region found earlier. Keeping T_{final} constant as preheat temperature i.e., 93 ℃, $T_{initial}$ ranging from 327 ℃ to 427 ℃ with 10 increments and ΔT ranging from 5 to 30 with 5 increments.

Table. 6 shows the standard deviation of the hardness values predicted throughout the built-up height at the middle potion of the model for all the combinations of $T_{initial}$ and ΔT. Standard deviation values which are less than 1.1 are highlighted. Less standard deviation represents less hardness variation so less standard deviation combination case gives the best uniformity. Similarly, the mean hardness values are tabulated in Table. 7 and the mean hardness values that are greater than 179 are highlighted. The critical values for standard deviation 1.1 and mean hardness value as 179 are considered just from observation. However, from Tables. 6 and 7 it is observed that some cases with reasonably positive standard variation have their mean hardness also less which is not the better option. The better option would be better mean hardness value with decent standard deviation. From Tables. 6 and 7, the best combination can be found as ΔT as 20 and $T_{initial}$ as 367 ℃.

The hardness range and the mean can be better visualised from the Fig. 31 which gives the information of hardness range and mean of all the layers for different $T_{initial}$ values at ΔT as 20. It is understood that optimum value to achieve better uniformity with decent hardness values can be achieved at 367 ℃. It is observed that the hardness range is increasing if $T_{initial}$ values are away from 367 ℃ at ΔT as 20. The mean hardness values are increasing with decrease in $T_{initial}$.

Table.6 Standard deviation of hardness values predicted along the built-up direction for 30 layers for different combinations of ΔT and $T_{initial}$

$T_{initial}$ (°C) \ ΔT	5	10	15	20	25	30
427	1.18	2.13	2.97	2.14	1.78	1.62
417	1.21	2.29	2.65	1.91	1.51	1.38
407	1.30	2.24	2.48	1.65	1.34	1.26
397	1.40	2.25	2.09	1.46	1.20	1.20
387	1.50	2.42	1.81	1.23	1.12	1.19
377	1.66	2.42	1.64	1.11	1.17	1.29
367	1.81	2.60	1.54	1.05	1.25	1.72
357	1.95	2.49	1.40	1.07	1.43	1.98
347	2.14	2.42	1.33	1.17	1.65	2.27
337	2.29	2.24	2.02	1.33	1.87	2.56
327	2.40	2.03	1.58	1.90	2.13	2.78

Table.7 Mean of hardness values predicted along the built-up direction for 30 layers for different combinations of ΔT and $T_{initial}$

| $T_{initial}$ (°C) \ ΔT	5	10	15	20	25	30
427	172.03	174.27	176.69	178.02	178.64	179.16
417	172.36	174.74	177.01	178.32	178.84	179.34
407	172.70	174.97	177.33	178.52	179.17	179.54
397	173.03	175.42	177.84	178.81	179.39	179.75
387	173.34	175.85	178.16	179.00	179.59	179.89
377	173.70	176.41	178.42	179.27	179.82	180.10
367	174.04	176.90	178.73	179.46	179.98	180.41
357	174.56	177.35	178.95	179.70	180.21	180.54
347	174.90	177.77	179.20	179.87	180.41	180.74
337	175.26	178.36	179.83	180.12	180.53	180.95
327	175.65	178.80	179.84	180.45	180.74	181.00
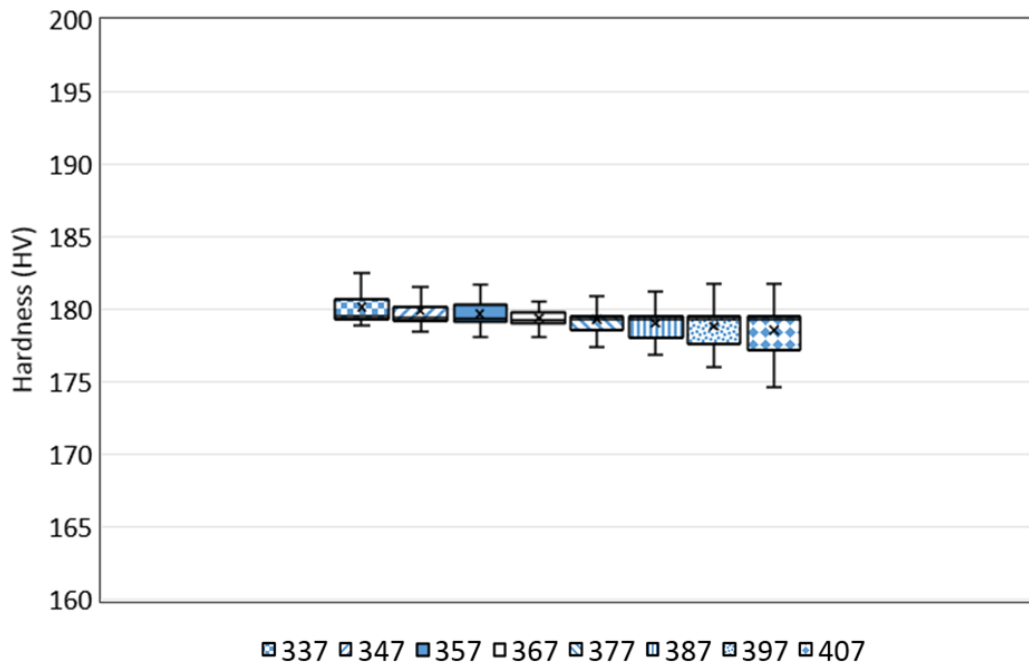
Fig. 31 Hardness range and mean for different T $_{initial}$ with ΔT as 20

Now keeping T$_{initial}$ at 367 ℃, various values of ΔT is examined. From Fig. 32, it can be seen that the hardness range and the mean is comparatively better for ΔT as 20.
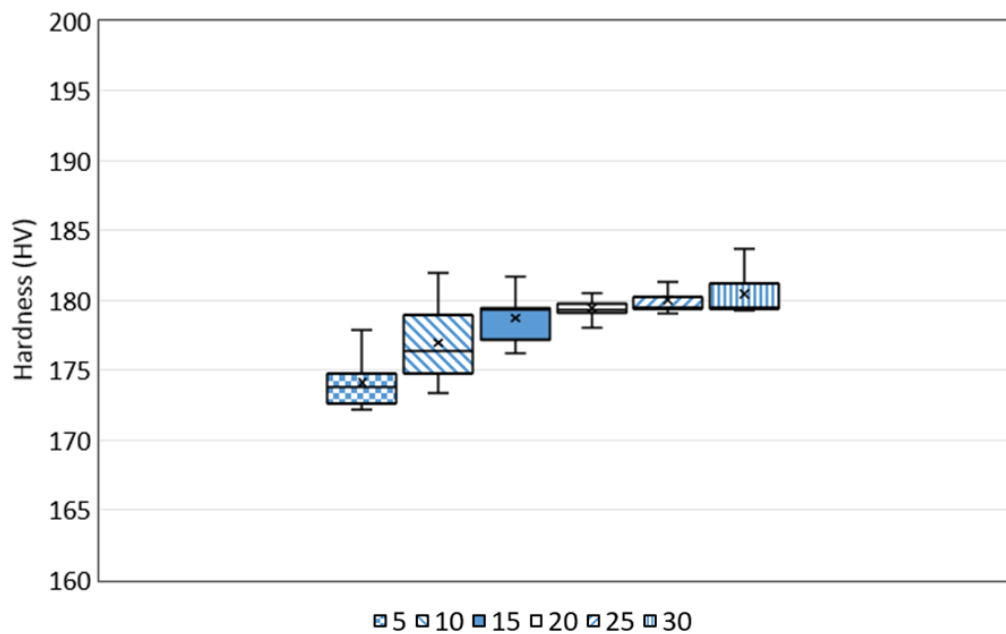

Fig. 32 Hardness range and mean for different ΔT at T $_{initial}$ as 367 ℃

The mean hardness values are increased with increase in ΔT till 15 after which it is almost constant. From above understanding it can be said that the better uniform hardness can be achieved at $T_{initial}$ as 367 ℃, T_{final} as 93 ℃ and ΔT as 20 for the considered parameters. $T_{initial}$, T_{final} and ΔT values may vary according to the geometric and process parameters. From the above understanding, it can be concluded that the present approach i.e., controlled cooling of heated baseplate while deposition gives uniform properties along built-up direction of the component. This approach is practically feasible by monitoring the temperature with the help of thermo-couple fixed at the bottom surface of the baseplate and controlling the deposition of each layer accordingly.

Some researchers [23, 47, 48, 50] found the hardness variation of steel AM components along the built-up direction, where they studied on less number of deposited layers. So, the effect of the baseplate and the effect of the varying thermal cycles separately are not able to explain properly. From this study, it is understood that the effect of baseplate remains till 10 layers after which its effect cannot be seen. Later in the top few layers variation of hardness is observed due to varying thermal cycles undergone by the region. The effect of baseplate on mechanical properties are comparatively higher than the variable thermal cycles. The proposed approach to achieve uniform properties is first of its kind. Hardness prediction is already proposed by Manvatkar [50] using different approach but the model is over predicting the actual hardness values. The current developed tool predicts the hardness which is in good agreement with experimental values.

Chapter 6

Conclusions and Future scope of work

From the experimental investigations performed to understand the mechanical property variation along the built-up direction and from various simulated outcomes to develop an understanding in achieving uniform mechanical properties, following conclusions are drawn,

- Cooling time and hardness plots gives the visualisation of the non-uniform property portions of the component. It can also be concluded from the current research that the bottom surface non-uniformity is due to substrate and the top portion is because of variable thermal cycles they undergone through.

- This thermal and hardness model provides a better platform to predict the hardness of layered manufactured components along built-up direction for certain range of mild steels.

- Hardness of the deposited layers can be controlled by controlling the baseplate temperature and the investigations on the approach of controlled diminishing of preheated baseplate temperature with layer wise deposition concludes the feasibility of achieving uniform mechanical properties.

- In the controlled diminishing baseplate temperature strategy, the initial temperature of heated baseplate and the temperature reduction layer wise plays a key role in achieving uniformity without softening the component.

The current study can give the scope to extend the work in the direction of,

- The current thermal model can be integrated with Mechanical model to investigate the formation of residual stress and the distortion in WAAM.

- Experimental investigations for the proposed schemes and predicting the formation of residual stresses and distortions.

- Studying the effects of various cooling strategies on mechanical properties by extending the current model.

References

[1]   W. E. Frazier, "Metal additive manufacturing: A review," J. Mater. Eng. Perform., vol. 23, no. 6, pp. 1917–1928, 2014.

[2]   H. Bikas, P. Stavropoulos, and G. Chryssolouris, "Additive manufacturing methods and modelling approaches: A critical review," Int. J. Adv. Manuf. Technol., vol. 83, no. 1–4, pp. 389–405, 2016.

[3]   Y. Zhang, Z. Wei, L. Shi and M. Xi "Characterization of laser powder deposited Ti–TiC composites and functional gradient materials," journal of materials processing technology, 206 438–444, 2008.

[4]   W. Ul, H. Syed, A. J. Pinkerton, and L. Li, "A comparative study of wire feeding and powder feeding in direct diode laser deposition for rapid prototyping," vol. 247, pp. 268–276, 2005.

[5]   Kim, Jae-Do, and Yun Peng. "Melt pool shape and dilution of laser cladding with wire feeding." Journal of Materials Processing Technology 104.3, 284-293, 2000.

[6]   Karunakaran, K. P., et al. "Rapid manufacturing of metallic objects." Rapid Prototyping Journal 18.4, 264-280, 2012.

[7]   A. A. Antonysamy, "Microstructure , Texture and Mechanical Property Evolution during Additive Manufacturing of Ti6Al4V Alloy for Aerospace Applications," p. 316, 2012.

[8]   D. Ding, Z. Pan, D. Cuiuri, and H. Li, "Wire-feed additive manufacturing of metal components: technologies, developments and future interests," Int. J. Adv. Manuf. Technol., vol. 81, no. 1–4, pp. 465–481, 2015.

[9]   S. W. Williams, F. Martina, A. C. Addison, J. Ding, G. Pardal, and P. Colegrove, "Wire + arc additive manufacturing," Mater. Sci. Technol., vol. 836, no. March, p. 1743284715Y.000, 2015.

[10] R. Baker, "Method of making decorative articles,"U.S. Patent 1533300, 1925.

[11] O. H. Eschholz, "Ornamental arc welding," U.S. Patent 1533239, 1925.

[12] H. K Shockey, "Machine for reclaiming worn brake drums," U.S. Patent 1886503, 1932.

[13] R. Carpenter Otis, and H. J. Ker, "Method and apparatus for metal coating metal pipes by electric fusion" U. S. Patent 2427350, 1947.

[14] P. M. Dickens, M. S. Pridham, R. C. Cobb, I. Gibson and G. Dixon, "Rapid prototyping using 3-D welding," Proc.Solid Freeform Fabrication Symp, DTIC Document, pp. 280 – 290, 1992

[15]   J. Schmidt, H. Dorner and E. Tenckhoff," manufacture of complex parts by shape welding", Journal of Nuclear Materials 171, 120-127, 1990.

[16] S. W. Williams, F. Martina*, A. C. Addison, J. Ding, G. Pardal and P. Colegrove," Wire+ Arc Additive Manufacturing" Materials Science and Technology, Vol.32, Iss, PP 641-647, 2016.

[17] H. Zhao, G. Zhang, Z. Yin, and L. Wu, "Effects of Interpass Idle Time on Thermal Stresses in Multipass Multilayer Weld-Based Rapid Prototyping," J. Manuf. Sci. Eng., vol. 135, no. 1, p. 11016, 2013.

[18] M. P. Mughal, H. Fawad, R. A. Mufti, and M. Siddique, "Deformation modelling in layered manufacturing of metallic parts using gas metal arc welding: effect of process parameters," Model. Simul. Mater. Sci. Eng., vol. 13, no. 7, pp. 1187–1204, 2005.

[19] M. P. Mughal, H. Fawad, and R. a Mufti, "Three-Dimensional Finite-Element Modelling of Deformation in Weld-Based Rapid Prototyping," Proc. Inst. Mech. Eng. Part C J. Mech. Eng. Sci., vol. 220, pp. 875–885, 2006.

[20] A. H. Nickel, D. M. Barnett, and F. B. Prinz, "Thermal stresses and deposition patterns in layered manufacturing," Mater. Sci. Eng. A, vol. 317, no. 1–2, pp. 59–64, 2001.

[21]   R. Ye, J. E. Smugeresky B. Zheng, Y. Zhoua and E. J. Lavernia," Numerical modelling of the thermal behaviour during the LENS process", Materials Science and Engineering A 428 ,47–53, 2006.

[22]   J. Yang and F. Wang," 3D finite element temperature field modelling for direct laser fabrication", Int J Adv Manuf Technol, 43,1060–1068, 2009.

[23]   Z. Jandric, M. Labudovic, and R. Kovacevic, "Effect of heat sink on microstructure of three-dimensional parts built by welding-based deposition," Int. J. Mach. Tools Manuf., vol. 44, no. 7–8, pp. 785–796, 2004.

[24]   Peyre, P., et al. "Analytical and numerical modelling of the direct metal deposition laser process." Journal of Physics D: Applied Physics 41.2, 025403, 2008.

[25]   Alimardani, Masoud, Ehsan Toyserkani, and Jan P. Huissoon. "A 3D dynamic numerical approach for temperature and thermal stress distributions in multilayer laser solid freeform fabrication process." Optics and Lasers in Engineering 45.12, 1115-1130, 2007.

[26]   C. Charles, Modelling microstructure evolution of weld deposited Ti-6Al-4V, PhD Thesis, Lulea University of Technology, 2008.

[27]   R. K. Chin, J. L. Beuth, and C. H. Amon, Thermomechanical modelling of molten metal droplet solidification applied to layered manufacturing, Mechanics of Materials, vol. 24, no. 4, pp. 257-271, 1996.

[28]   R. K. Chin, J. L. Beuth, and C. H. Amon, Successive Deposition of Metals in Solid Freeform Fabrication Processes, Part 1: Thermomechanical Models of Layers and Droplet Columns, Journal of Manufacturing Science and Engineering, vol. 123, no. 4, pp. 623-631, 2001.

[29]   R. K. Chin, J. L. Beuth and C. H. Amon, Successive Deposition of Metals in Solid Freeform Fabrication Processes, Part 2: Thermomechanical Models of Adjacent

Droplets, Journal of Manufacturing Science and Engineering, vol. 123, no. 4, pp. 632-638, 2001.

[30] Ding, J. "Thermo-mechanical analysis of wire and arc additive manufacturing process." ,2012.

[31] J. Ding et al., "Thermo-mechanical analysis of Wire and Arc Additive Layer Manufacturing process on large multi-layer parts," Comput. Mater. Sci., vol. 50, no. 12, pp. 3315–3322, 2011

[32] L. Zhang and P. Michaleris, "Investigation of Lagrangian and Eulerian finite element methods for modeling the laser forming process," Finite Elem. Anal. Des., vol. 40, no. 4, pp. 383–405, 2004.

[33] P. Michaleris, "Modeling metal deposition in heat transfer analyses of additive manufacturing processes," Finite Elem. Anal. Des., vol. 86, pp. 51–60, 2014.

[34] H. Zhao, G. Zhang, Z. Yin, and L. Wu, "A 3D dynamic analysis of thermal behavior during single-pass multi-layer weld-based rapid prototyping," J. Mater. Process. Technol., vol. 211, no. 3, pp. 488–495, 2011.

[35] Dickens, P. M., Cobb, R. C., Gibson, I. and Pridham, M. S., Rapid prototyping using 3D welding, Journal of Design and Manufacturing, **3**(1), p. 39-44, 1992.

[36] Y. A. Song, S. Park, D. Choi and H. Jee, 3D welding and milling: Part I-a direct approach for freeform fabrication of metallic prototypes, International Journal of Machine Tools and Manufacture, 45(9), p. 1057-1062, 2005.

[37] K. P. Karunakaran, S. Suryakumar, V. Pushpa and S. Akula, Retrofitment of a CNC machine for hybrid layered manufacturing, International Journal of Advanced Manufacturing Technology, 45(7-8), p. 690-703, 2009.

[38] W. Aiyiti, W. Zhao, B. Lu, and Y. Tang, "Investigation of the overlapping parameters of MPAW-based rapid prototyping," Rapid Prototyp. J., vol. 12, no. 3, pp. 165–172, 2006.

[39]   S. Suryakumar, K. P. Karunakaran, A. Bernard, U. Chandrasekhar, N. Raghavender, and D. Sharma, "Weld bead modeling and process optimization in Hybrid Layered Manufacturing," CAD Comput. Aided Des., vol. 43, no. 4, pp. 331–344, 2011.

[40]   Y. Cao, S. Zhu, X. Liang, and W. Wang, "Overlapping model of beads and curve fitting of bead section for rapid manufacturing by robotic MAG welding process," Robot. Comput. Integr. Manuf., vol. 27, no. 3, pp. 641–645, 2011.

[41]   J. Xiong, G. Zhang, H. Gao, and L. Wu, "Modeling of bead section profile and overlapping beads with experimental validation for robotic GMAW-based rapid manufacturing," Robot. Comput. Integr. Manuf., vol. 29, no. 2, pp. 417–423, 2013.

[42]   J. Xiong, G. Zhang, Z. Qiu and Y. Li," Vision-sensing and bead width control of a single-bead multi-layer part: material and energy savings in GMAW-based rapid manufacturing", Journal of Cleaner Production 41 ,82-88, 2013;

[43]   J. D. Spencer, P. M. Dickens, and C. M. Wykes, "Rapid prototyping of metal parts by three-dimensional welding," Proc. Inst. Mech. Eng. Part B J. Eng. Manuf., vol. 212, no. 3, pp. 175–182, 1998.

[44]   F. Martina: 'Investigation of methods to manipulate geometry, microstructure and mechanical properties in titanium large scale wire + arc additive manufacturing'; PhD thesis, Cranfield University, UK, Cranfield, UK 2014.

[45]   E. Brandl, B. Baufeld, C. Leyens, and R. Gault, "Additive manufactured Ti-6A1-4V using welding wire: Comparison of laser and arc beam deposition and evaluation with respect to aerospace material specifications," Phys. Procedia, vol. 5, no. PART 2, pp. 595–606, 2010.

[46]   E. Brandl, A. Schoberth, and C. Leyens, "Morphology, microstructure, and hardness of titanium (Ti-6Al-4V) blocks deposited by wire-feed additive layer manufacturing (ALM)," Mater. Sci. Eng. A, vol. 532, pp. 295–307, 2012.

[47]   L. Costa et al. "Rapid tooling by laser powder deposition: Process simulation using finite element analysis." Acta Materialia 53.14, 3987-3999, 2005.

[48]   H.E. Kadiri, L. Wang, M.F. Horstemeyer, R.S. Yassar, J.T. Berry, S. Felicelli and P. T. Wang," Phase transformations in low-alloy steel laser deposits", Materials Science and Engineering A 494 ,10–20, 2008.

[49]   B. Zheng et al. "Thermal behaviour and microstructure evolution during laser deposition with laser-engineered net shaping: part II. Experimental investigation and discussion." Metallurgical and Materials Transactions A39.9: 2237-2245, 2008.

[50]   V. D. Manvatkar et al. "Estimation of melt pool dimensions, thermal cycle, and hardness distribution in the laser-engineered net shaping process of austenitic stainless steel." Metallurgical and materials transactions A 42.13: 4080-4087, 2011.

[51]   A. Sharma, N. Arora, and S. R. Gupta, "Investigation into Arc Behavior during Twin-Wire Submerged Arc Welding," Mater. Manuf. Process., vol. 25, no. 8, pp. 873–879, 2010.

[52]   R. L. Ule, Y. Joshi, and E. B. Sedy, "A new technique for three-dimensional transient heat transfer computations of autogenous arc welding," Metall. Trans. B, vol. 21, no. 6, pp. 1033–1047, 1990.

[53]   J. Trzaska, "Empirical Formulas for the Calculations of the Hardness of Steels Cooled from the Austenitizing Temperature," Arch. Metall. Mater., vol. 61, no. 3, pp. 1297–1302, 2016.